LASER RANGING USING INCOHERENT PULSE COMPRESSION TECHNIQUES

DANIEL GRODENSKY

FACULTY OF ENGINEERING

PH.D. THESIS

Submitted to the Senate of Bar-Ilan University

RAMAT-GAN, ISRAEL **OCTOBER 2014**

THIS WORK WAS CARRIED OUT UNDER THE SUPERVISION OF PROF. AVI ZADOK FROM THE FACULTY OF ENGINEERING AT BAR-ILAN UNIVERSITY

Acknowledgments

First, I would like to thank my advisor, Prof. Avi Zadok, for the opportunity to be part of his research group and to work on very interesting research projects during the course of the study. Avi has inspired me to take this challenge and was always nearby to help and give a clever advice. His dedication, his close relations with his students is something that is not common and requires a lot of patience and dedication. I never forget late night hours that we spent together in the university corridors trying to collimate the laser beam at long range distances.

Avi's guidance, insight and possibility to catch in a moment nature of sophisticated problems are hard to overestimate. I am extremely grateful to Avi for the opportunity to be his student.

I would like to thank Daniel Kravitz, who is my close friend. We have been working closely together on the first part of the research since me joined Avi's group. Daniel is talented researcher and good professional. I am glad that I had the opportunity to work with Daniel side by side during my academic study.

Especially I would like to thank Nadav Arbel, who worked with me on the second part of the research. His diligence and devotion helped me to finish the study and I am grateful to him for that.

I wish to thank Dr. Arkady Rudnitsky who helped a lot during the research and gave many suggestions how to improve the system performance.

I wish to thank also Mrs. Dina Yeminy, for her responsiveness, support and help since joining the Faculty of Engineering 5 years ago.

In addition, I would also like to thank Prof. Nadav Levanon for collaborating with us and introducing us the magic world of radar signals.

Last but not least, I thank my family. My wife Inna, my mother-in-law Ella and my kids: Nathanel, Ariel, Eyal and little Dana, for their support, encouragement and great patience throughout my study.

Table of Contents

Page

List of Figures

Page

List of Tables

List of symbols

B	Bandwidth
B_N	Noise bandwidth
c	Speed of light
$c[n]$	Bipolar code of length N
D	Spatial resolution
dA	Target surface area
D_t	Circular transmitter aperture
D_r	Circular receiver aperture
E	Signal energy
F	EDFA noise figure
f_{IF}	Intermediate frequency
f_{LO}	Local oscillator frequency
G	EDFA power gain
$h(t)$	Impulse response
$i_N(t)$	Noise current
$i_D(t)$	Deterministic current
$s(t)$	Signal
M	Number of phases in phase-coded waveform
L	Code length
N	Code length (in Chapter 1, section 1.2)
N	Number of applied average processes (in Chapter 1, section 1.5)

N_0	Noise power per unit bandwidth
P_{PD}	Photo-detector noise power
P_{RIN}	RIN noise power
P_{CW}	Continuous wave power
P_t	Transmitted power
P_r	Received power
R	Matched reference
$\tilde{R}$	Miss-matched reference
T	Transmission sequence (Chapter 2, section 2.6)
T	Width of main correlation peak (Chapter 1, section 1.2)
T_p	(Sub) pulse length in phase-coded waveform
α	Loss
Δf_{IF}	Pass-band filter bandwidth
$\Delta\varphi$	Phase difference
Δt	Time interval
δ	Delta function
λ	Wavelength
θ	Angle of incident
θ_t	Laser beam angular divergence
θ_R	Target surface angular dispersion
π	Pi number equal to 3.14159…
ρ_t	Target reflectance parameter

σ_N	Noise RMS bandwidth
σ_R	Ranging accuracy
τ	Delay
τ_L	Coupling loss factor
$°K$	Kelvin degree

List of Abbreviations

ADC	Analog to Digital Converter
AGC	Automatic Gain Control
AM	Amplitude Modulation
APD	Avalanche Photo-Diode
ASE	Amplified Spontaneous Emission
AWG	Arbitrary Waveform Generator
BOTDA	Brillouin Optical Time Domain Analysis
BW	Bandwidth
CW	Continuous Wave
DB	Decibel
DBG	Dynamic Brillouin Gratings
DC	Direct Current
DFB	Distributed Feedback Laser
ESNR	Electrical Signal to Noise Ratio
EDFA	Erbium Doped Fiber Amplifier
FM	Frequency Modulation
FPA	Focal Plane Array
FO	Fiber Optic
FOV	Field of View
FWHM	Full Width at Half Maximum
IF	Intermediate Frequency
InGaAsP	Indium Gallium Arsenide Phosphide
ISLR	Integrated Sidelobe Ratio
LADAR	Laser Radar

LFM	Linear Frequency Modulation
LiDAR	Light Detection and Ranging
LO	Local Oscillator
LPI	Low Probability of Intercept
M-Factor	Multiplication Factor
MEMS	Micro Electro Mechanical System
MMA	Micro Mirror Array
MPSL	Minimum Peak Sidelobe Level
MZM	Mach Zehnder Modulator
NEP	Noise Equivalent Power
NF	Noise Figure
NIST	National Institute of Standards and Technology
NIR	Near Infra Red
NLFM	Non Linear Frequency Modulation
OSNR	Optical Signal to Noise Ratio
OTDR	Optical Time Domain Reflectometry
PIN	P type – Intrinsic – N type
PRI	Pulse Repetition Interval
PRR	Pulse Repetition Rate
PSLR	Peak to Sidelobe Ratio
RADAR	Radio Detection and Ranging
RIN	Relative Intensity Noise
RF	Radio Frequency
RMS	Root Mean Square
SMMA	Scanning Micro Mirror Array
SNR	Signal to Noise Ratio

SOA	Semiconductor Optical Amplifier
ToF	Time of Flight
T/R	Transmit / Receive
VGA	Video Graphics Array
WDM	Wavelength Division Multiplexing
WLAN	Wireless Local Area Network
0D	Zero Dimensional (single point)
2D	Two Dimensional
3D	Three Dimensional

List of Publications

Book Chapter:

1. A. Zadok, D. Grodensky, D. Kravitz, Y. Peled, M. Tur, X. Wu and A. E. Willner, "Ultra-Wideband Waveform Generation Using Nonlinear Propagation in Optical Fibers," *in Ultra Wideband Communications: Novel Trends - Antennas and Propagation*, Mohammad Matin (Ed.), Intech, 2011.

Journal papers:

1. D. Grodensky, D. Kravitz, and A. Zadok, "Ultra-Wideband Microwave-Photonic Noise Radar Based on Optical Waveform Generation," *IEEE Photonics Technology Letters*, vol. 24, pp. 839–841, 2012.
2. D. Kravitz, D. Grodensky, N. Levanon, and A. Zadok, "High-Resolution Low-Sidelobe Laser Ranging Based on Incoherent Pulse Compression," *IEEE Photonics Technology Letters* vol. 24, pp. 2119-2121, 2012.

Conference papers:

1. D. Grodensky, D. Kravitz, and A. Zadok, "Ultra-Wideband Noise Radar Based on Optical Waveform Generation," Proceedings of IEEE Conference on Microwaves, Communications, Antennas and Electronic Systems (COMCAS) 2011, Tel-Aviv, Israel, Dec. 2011.
2. D. Grodensky, D. Kravitz, and A. Zadok, "Ultra-Wideband Noise Radar Based on Optical Waveform Generation," Proceedings of SPIE conference on Radar Sensor and Technology, SPIE, Defense Security and Sensing 2012, Baltimore MD. Proc. SPIE 8361, 8361-43, 2012
3. D. Kravitz, D. Grodensky, A. Zadok, and Levanon, N., "Incoherent compression of complementary code pairs for laser ranging and detection," Proceedings of IEEE International Conference on Microwaves, Communications, Antennas and Electronics Systems (COMCAS) 2013, Tel-Aviv, Israel, Oct. 2013.
4. D. Grodensky, D. Kravitz, N. Arbel, N. Levanon and A. Zadok, "Incoherent pulse compression in laser range finder", Proceedings of SPIE conference on Laser Radar Technology and Applications XIX; and Atmospheric Propagation XI, 90800M, Baltimore MD. Proc. SPIE 9080, June 2014.

Abstract

High resolution ranging systems are of great importance for both civilian and military applications. In comparison to radio frequency (RF) waveforms, the optical waveforms used in laser detection and ranging (a.k.a. LADAR) can carry broader bandwidth signals and thus provide better range resolution. They also provide better immunity to electromagnetic interference, and are readily integrated with fiber-optic distribution.

High range resolution can be obtained using short and intense pulses. However, the transmission and processing of such pulses is difficult and potentially unsafe. In addition, the overall signal energy falls off with the use of short pulses, and the signal to noise ratio (SNR) of collected echoes is thus degraded. Instead, temporally extended waveforms or sequences, in conjunction with proper compression techniques at the receiver end, may be used. The auto-correlation, or matched-filtering, of long waveforms and sequences effectively compresses their entire energy into an intense and narrow virtual peak with low residual sidelobes. Such sequences may therefore reproduce the high resolution and low background that are provided by a short and high-power single pulse, with significant added values: the instantaneous power of the extended waveforms can be orders-of-magnitude lower, making them safer and simpler to generate in a real-world system and more difficult to intercept by an adversary.

The objective of this work is high resolution laser ranging measurements using compression of long waveforms. The proposed LADAR system employs an encoded sequence of pulses and proper post-processing to obtain high resolution ranging measurements with low sidelobes. In most scenarios, effective compression requires

phase coding, whereas intensity coding leads to inferior performance. The measurement of phase in a photonic system, however, involves complicated coherent receivers. Alternatively, we employ a novel incoherent compression scheme, which was previously proposed by Prof. Nadav Levanon of Tel-Aviv University. In this scheme, binary phase sequences are converted to a unipolar, intensity modulation representation through a position-coding algorithm, and then used to modulate the laser ranging source. Reflected echoes undergo simple direct detection, followed by correlation with a bipolar reference sequence that is digitally stored at the receiver. Even though both transmit and receive operation are incoherent, the filtered sequence nearly replicates the effective sidelobe suppression of the original phase code.

Laser range finding using incoherent compression was demonstrated experimentally. Unipolar representations of two types of codes were examined: 1) minimum peak to sidelobe (MPSL) sequences, and 2) complementary code pairs (a.k.a. Golay codes), whose correlation sidelobes ideally cancel out. A ranging resolution of 15 cm at 70m distance was demonstrated using this system. The range to a target could be observed at poor electrical SNRs, as low as -20 dB. The measurement range depends on the reflectance of targets, transmitted optical power, receiver aperture and code length, and could reach hundreds of meters and even a kilometer. The results provide the first successful demonstration of the incoherent compression principle using echoes that are reflected from a realistic, Lambertian target.

The work is organized as follows. A general introduction to sequence compression and LADAR systems is given in Chapter 1. Relevant literature surveys on the relative merits of different coded waveforms are highlighted in this chapter. A laser ranging system based on incoherent pulse compression, alongside simulations

and preliminary short-range lab experiments, is described in Chapter 2. Chapter 3 is dedicated to a laser ranging measurements to a realistic Lambertian reflecting target, using the incoherent pulse compression of various sequences. Concluding remarks, a critical discussion of system performance and a comparison between time-of-flight and sequence compression approaches are provided in Chapter 4. Future work and perspective are also suggested at the end of this chapter.

CHAPTER

1

Introduction

1.1 Laser Radar Background

RADAR (**RA**dio **D**etection **A**nd **R**anging) is the process of transmitting, receiving, detecting, and processing an electromagnetic wave that is reflected from a target. Early RADAR experiments began in the late 19th century, and a first system was developed by the German Army in 1935 [1]. As theoretical and technical developments continued, RADAR techniques and applications expanded into almost every aspect of the modern world.

Pulsed light sources and optical detectors were first used in 1938 to measure the base heights of clouds [2]. The acronym LiDAR (**LI**ght **D**etection **A**nd **R**anging) was first used in 1953, [3] and development of high-energy or Q-switched pulsed lasers in 1962 made such sources available for LiDAR applications. In 1963, Fiocco and Sullivan published work on atmospheric observations using a Ruby laser [4]. Since that time, laser-based sensors have demonstrated most, if not all, of the same functions as radio frequency (RF) or microwave RADARs.

All ranging systems, whether RADAR, LiDAR, or LADAR ((**LA**ser **D**etection **A**nd **R**anging), function by transmitting and receiving electromagnetic energy. The only difference among them is that they work in different frequency bands [5].

Therefore, many of the same considerations, such as antenna theory and propagation time, apply to all of these systems.

While many waveforms are used in both RADAR and LADAR: continuous-wave (CW), amplitude-modulated (AM), frequency-modulated (FM) or pulsed, the mechanisms for producing these waveforms in LADAR and RADAR are significantly different. Producing the desired waveform in a RADAR transmitter could be as simple as turning an oscillator (or amplifier) on and off. In comparison, the various LADAR waveforms are often created by operating on the optical path of the laser. Q-switches that can rapidly change the output coupling of the cavity are used to dump the built-up energy stored in the cavity, producing a sharp, short pulse. Components such as modulators are used to impress modulation on the laser output. Because the optical alignment of these components is critical, care must be taken to provide very stable bases and mounts for the optical elements. The development of fiber-optic-based components has made LADAR elements more closely analogous to their counterparts in RADAR systems [16].

Once a signal is generated, it must be launched towards potential targets. In RADAR, this is done through an antenna. While RADAR could operate with a simple dipole-type antenna, the resulting omnidirectional beam pattern would be of minimal use, so some type of directivity is needed using more elaborate antenna designs. The optical equivalent of the antenna in a LADAR system is a telescope or an arrangement of optical lenses. The simplest system to implement is the *bi-static* configuration shown in Fig. 1.1(a). Here, separate paths and antennas are used for the transmission and receiving functions. Although this configuration is mechanically simple, it does result in a larger system package, especially for some of the longer-wavelength RADAR systems. The main advantage of this configuration is that it does not involve

the coupling of the noise produced by the antenna's backscattering of the transmitted beam into the receiver channel. This configuration is rarely used in modern RADAR systems, but it is commonly used in LADAR systems. For most current RADAR applications, the same antenna is used for both the transmission and receiving functions in a so-called a *mono-static* configuration, Fig. 1.1(b).

While using this configuration can reduce the size and mechanical complexity of the system, it does increase the complexity of internal circuitry and subsystems. The use of only one antenna requires the incorporation of a transmit/receive (T/R) switch. The switch is a directional device that routes the energy coming from one port to the next in a rotating direction, e.g., energy coming from the transmitter is routed to the antenna, whereas energy from the antenna is routed to the receiver. Ideally, only marginal energy (cross-talk) is routed in the reverse direction. In microwave systems, this switch is called a *circulator*, and a magnetic field in the waveguide effects the signal rotation around the signal path. In a LADAR system, a common T/R switch uses waveplates to rotate the polarization of the laser beam and a polarization sensitive beamsplitter to route the energy into the proper channel. A fiber-coupled circulator is a directly analogous to the microwave waveguide and circulator.

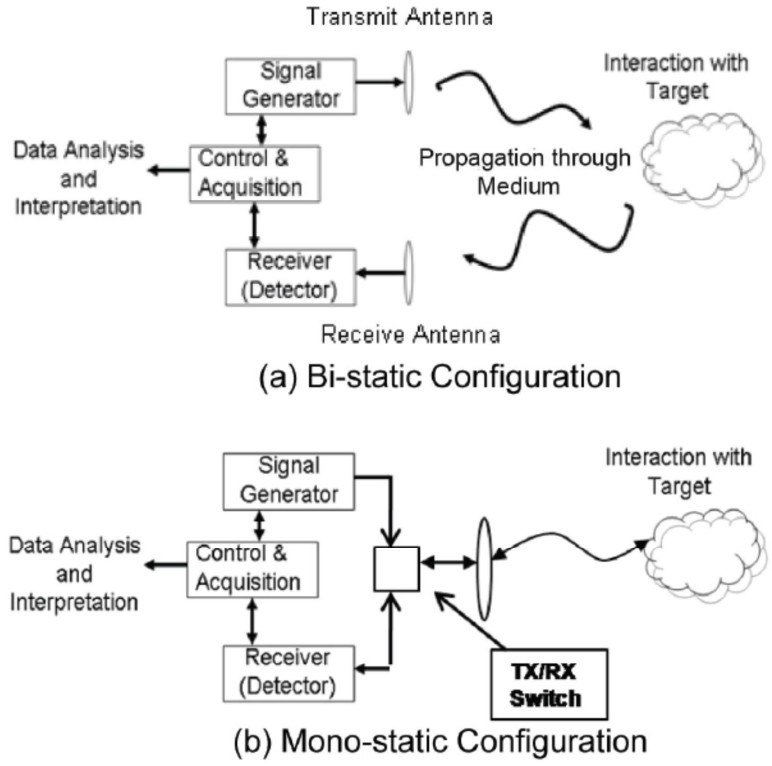

Figure 1.1 Typical LADAR/RADAR systems. [16]

The final subsystem shown in Fig. 1.1 is the receiver. For both RADAR and LADAR systems, the receiver function is to transform the propagating energy captured by the antenna into an electrical signal that can be processed to extract the desired information. In a RADAR system, the fluctuating electromagnetic fields of the returning signal induce currents in the receiver that can be picked up by the detector and amplified, thus creating the signal to be processed by subsequent subsystems [16]. In a LADAR system, the returning photons cannot directly induce this type of current. Instead, a photodiode is used to convert the photons to current. Charge carriers are generated in response to light incident upon the photodiode, and the photon energy of received light is converted into an electrical signal by releasing and accelerating current-conducting carriers within the semiconductor. This light-

induced current of the photodiode is proportional to the intensity of the incident radiation and forms the signal that is transferred to other subsystems within the receiver. Therefore, if phase information is required in a LADAR, then mixing with a phase-locked local oscillator (LO) is required upon detection (i.e. a *coherent receiver*) [16].

For most modern RADAR systems, the targets of interest are usually smaller than the transmitted beam width, so that the targets act as isotropic scatterers. On the other hand, LADAR systems often have beam widths smaller than the targets, and the targets can resemble anything from a Lambertian to a specular reflector and often are combinations of both. Except for a few bands around 22.2, 60, and 94 GHz, most RADAR systems are not affected by the same atmospheric absorption attenuation that affects LADAR. In general, the following comparisons can be stated for LADAR and RADAR systems:

- Optically thick clouds and precipitation can attenuate a LADAR beam, while RADAR scatterers may consist of clouds and hydrometeors (e.g., rain or frozen precipitation). Thus, RADAR systems are generally less susceptible to atmospheric absorption effects than LADAR systems.
- LADAR beam divergence can be two to three orders of magnitude smaller than conventional 5- and 10-cm-wavelength RADAR. This gives LADAR systems superior spatial resolution but a less efficient wide-area search capability than a RADAR system.
- The combination of the short pulse (possibly on ps scale), and the small beam divergence (about 10^{-3} to 10^{-4} rad), creates small illuminated volumes for LADAR. This makes LADAR better at conducting measurements in confined spaces such as urban areas.

1.1.1 *Resolution and signal-to-noise ratio*

RADAR and LADAR are integral parts of many modern weapon systems. Their ability to work at long ranges is incomparable with any other existing sensors. Use of advanced signal processing techniques has greatly enhanced the detection probability and resolution characteristics of the modern RADAR/LADAR systems. The capabilities of wideband/high-resolution RADAR and LADAR in target detection, recognition and analysis of the backscattering media, have increased their role in many areas of defense and civil applications. Most of the civil applications are concentrated on remote sensing, investigation of natural resources, ground mapping and high-resolution imaging of objects; the applications of military systems include intelligence, surveillance, navigation, detection, recognition, guidance of weapons, battle field surveillance, anti-aircraft fire control etc. [6-7].

Target detection and parameter estimation become difficult practical problems of interest when the target is small and/or is at a long distance. In addition, another practical aspect also comes into picture, when the performance characteristics are discussed, namely the *resolution*. In general, the resolution can be defined in terms of system capability to distinguish a desired target in a multi-target environment. The detection and estimation problems become quite challenging when the target is located in a multiple target scenario, where interference from several targets needs to be addressed. Resolution thus becomes a critical parameter of interest in all discussions related to modern high performance systems [8-9].

Another key parameter in the detection of the target and the extraction of the desired information is the signal-to-noise ratio (SNR), which is defined as the ratio between the power of the peak signal and the average noise power [10]. The SNR can be optimized in a *matched-filter receiver*, for which the SNR can be shown to be

given by $2E/N_0$, where E is received signal energy and N_0 is noise power per unit bandwidth [10-11]. The ranging system detection capability thus becomes a function of the energy associated with the received signal [10, 12].

To achieve high energy content in transmitted signal, either the peak transmitted power may be increased for a given pulse duration, or an elongated pulse length may be used for a given peak power [10]. As most of the transmitters are operated near peak power limitations [13], the energy content may only be increased when a long duration pulse is transmitted. On the other hand, high range resolution requires short pulses. Due to these contrary needs, of long pulses for detection and of short pulses for range resolution, early ranging systems faced difficulties in achieving the two functions simultaneously [13]. Both design objectives can be successfully met by using pulse compression techniques, as will be described in the next part (1.2).

1.1.2 *Incoherent and coherent LADAR systems*

In general, two types of LADAR systems exist: incoherent, which rely on direct detection of intensity only, and coherent, which make use of both the amplitude and the phase information of the optical wave. The differences between the two are illustrated in Fig. 1.2. In coherent systems, a fraction of the outgoing laser energy is split off and redirected to the receiver detector. This energy is then aligned with the collected LADAR echoes on a photo-detector, which is operating as a classical mixer. Generally speaking, coherent LADARs can operate at lower SNRs than their incoherent counterparts [14]. In addition, coherent systems generally allow for better use of sequence compression techniques [15], which rely for the most part on frequency and phase coding. Sequence compression will be addressed in much detail later in this thesis.

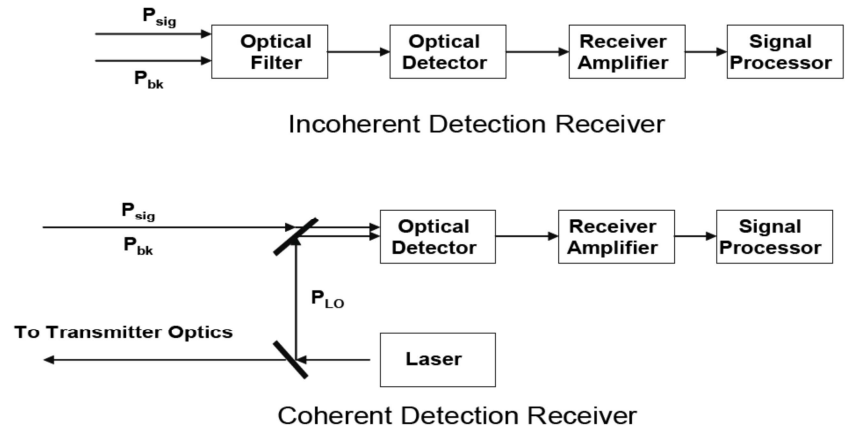

Figure 1.2 Block diagrams of incoherent (top) and coherent (bottom) LADAR systems [16].

While prevalent in RF and microwave systems, coherent receivers in the optical domain come at a cost of significant complexity [14]. An intermediate and highly appealing approach, which will be explored in this research, is the direct detection of pulse position modulated sequences. A proper post-detection processing of such sequences could allow for highly effective compression, which could rival those of coherent systems.

1.1.3 *LADAR applications*

LADAR systems can be catalogued into many categories. They may be grouped according to their transmitted waveform (i.e., CW, continuously-modulated, or pulsed); by receiver concept (coherent or direct detection); or by the intended measurement (range, velocity, backscatter, or spectral absorption). Development of LADAR systems is advancing rapidly [16]. Their applications include range-finders [17], 2D and 3D imaging systems [18], Doppler vibrometers [19], and synthetic aperture imaging [19-20]. Three-dimensional images are valuable in applications such as mapping, target recognition and machine gesture control. A 3D image of a scene is constructed using combined multiple range measurements taken along different lines of sight. Traditional 3D LADAR systems use scanning mirrors in order to obtain high

resolution images. In order to measure Doppler shifts, coherent receivers are needed. These coherent LADARs are sensitive enough to measure surface vibrations of remote objects on nanometirc scale [19]. Despite this impressive growth in such relatively recent LADAR applications, the primary objective of LADAR remains the measurement of the range to a target.

1.1.4 *Common ranging measurements techniques*

The most commonly-used LADAR scheme relies on the transmission of short and intense isolated pulses, and time of flight (ToF) measurements of collected reflections [16]. Laser pulses created by Q-switched systems can have durations on the order of nanoseconds. The receiver calculates the time it took a single pulse to make a round trip to the target and back. This time equals to the roundtrip distance divided by the speed of light.

A block diagram of a ToF LADAR range finder is shown in Fig.1.3 (left). This system consists of a laser transmitter emitting pulses with a duration of few ns, a receiver channel including a PIN or an avalanche photodiode (APD), amplifiers, an automatic gain control (AGC) and timing discriminators. The emitted light pulse (start pulse) triggers the time interval measurement unit, and the reflected light pulse (stop pulse) stops it. In this concept range accuracy and precision are limited by the length of the transmitted laser pulse, the pulse's shape, receiver electronics and noise sources in the LADAR system. In order to get a significant working distance, intense and short pulses are needed.

Another ranging measurement technique is based on *RF phase-shifts*. In a phase-shift range-finder, the optical power is modulated with a constant radio frequency. The basic operating scheme of the device is shown in Fig.1.3 (right). A

sine wave of frequency f_{RF} is generated by the main oscillator and modulates the DC current of the laser diode. After reflection from the target, a photodiode collects a part of the laser beam. Measurement of the distance D is deduced from the RF-domain phase difference between the photo-detected current and the original out-going signal. In this technique the accuracy and precision are limited by drifts in the intermediate frequency f_{IF} (see figure), cross-talk between transmitter and receiver channels, and signal distortions.

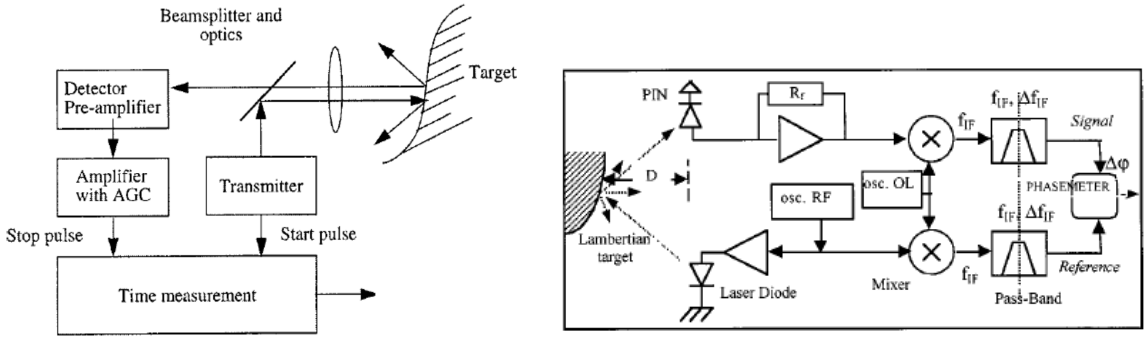

Figure 1.3 Left: block diagram of ToF LADAR range finder [17]. Right: block diagram of phase-shift LADAR rangefinder [17]. D: Distance. PIN: PIN photo-diode. $osc.RF$: RF oscillator. $osc.OL$: Local oscillator. f_{IF}: Intermediate frequency. Δf_{IF}: Pass-band filter bandwidth. $\Delta\varphi$: phase difference.

Another common technique for ranging measurements is based on linear frequency modulation (LFM) of the laser signal [21-22] and a coherent receiver. The basic concept of an LFM LADAR is illustrated in Fig. 1.4. The driving current to a laser diode source is being modulated by a ramp waveform, resulting in a periodic linear frequency chirp. The laser output is launched simultaneously towards the object and towards a reference mirror using a beam splitter. The reflected signals are then superimposed in a square-law detector. The beating term, which is oscillating at some intermediate frequency f_{IF}, is further amplified and measured with a frequency counter. The intermediate frequency f_{IF} is proportional to the time delay between the

transmitted and received waveforms. Thus, with the a-priori knowledge of the sweep bandwidth and repetition rate of the LFM waveform, the distance to the target can be obtained.

Due to the square law mixing process, the amplitude of the detector output at f_{IF} is proportional to the amplitudes (as opposed to the power levels) of both the collected echo signal and the reference. Accordingly, the dynamic range of the frequency-swept technique is twice as large (in dB scale) as that of pulsed radars, in which the electrical signal is proportional to the power collected from the object. The improvement in dynamic range in turn extends the total working distance.

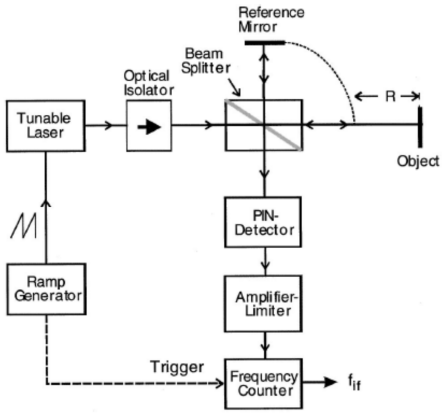

Figure 1.4 Block diagram of LFM based LADAR range finder [17].

The limiting factor of swept-frequency LADAR systems is the nonlinear frequency response of laser diodes. The frequency modulation response of a laser diode is, in general, non-uniform, so that a linear optical frequency sweep cannot be perfectly realized by ramp modulation of the control current. As a consequence, deviations from the linear sweep usually occur, and in turn lead to variations in the intermediate frequency f_{IF}. Another fundamental limitation of the measurement accuracy is due to the phase noise of the laser diode [23-24]. Frequency-modulated laser diodes with narrow spectral linewidths are in general preferable for highly accurate range measurements.

1.1.5 *Sources of noise in LADAR systems*

Several phenomena contribute noise to LADAR measurements. The noise sources include statistical fluctuations in the amount of light arriving at the LADAR detector (for example due to relative intensity noise, RIN, of the laser diode source); variations in the photo-detected current that are due to the quantum-mechanic characteristics of the detection process (*Shot noise*); thermal noise due to fluctuations in current along electrical conductors; speckle patterns, and additive stray photons.

Shot noise is inherent to the detection process. Due to the particle nature of light, the number of photo-electrons counted during a time interval Δt is a random variable, even if the incident optical intensity is entirely deterministic. Figure 1.5 demonstrates the effect of random photon arrival times on the number of photons counted by a detector with a finite integration time. The mean number of photo-electrons is proportional to the expected number of photons as decreed by the incoming intensity and measurement duration. The number of photo-electrons measured during the detector integration time is characterized by Poisson statistics [14]. The standard deviation, according to these statistics, is proportional to the square root of the mean value. Therefore, in those systems in which shot noise is the performance-limiting mechanism, the SNR can be improved by elevating the source power.

Noise currents flow in any conductor that is not at 0 °K. Thermal noise relates to the fact that at a finite temperature, electrons move randomly in the conductor. Random thermal motion of electrons in a resistor manifests as a fluctuating current, even in the absence of an applied voltage. The load resistor in the front end of an optical receiver adds such fluctuations to the current generated by the photodiode. Thermal noise is independent of the incoming power. The effect of thermal noise is

often quantified through a quantity called the noise-equivalent power (NEP), defined as the minimum optical power per unit bandwidth required for an SNR of unity. As in the shot noise-limited case, the SNR of a thermal noise-limited system improves with incoming power.

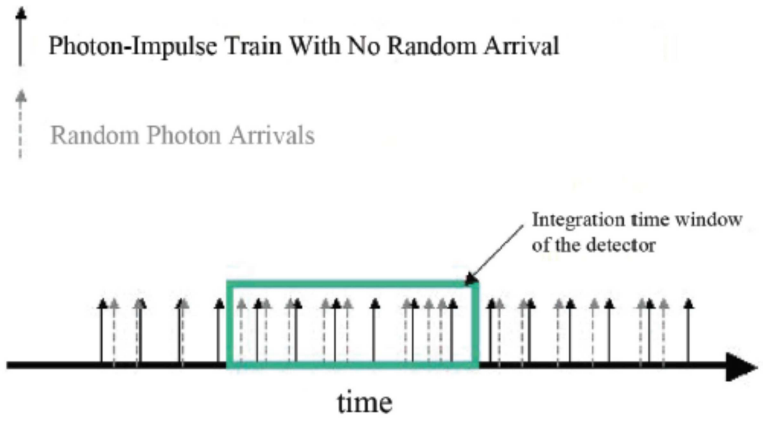

Figure 1.5 Effect of random arrival times on the number of photons counted during a fixed interval. If the photons arrive at predictable intervals, six photons are counted. Random arrival times here show eight photons being counted. [16]

The output of a semiconductor laser exhibits fluctuations in its intensity, phase, and frequency, even when the laser is biased at a constant current with negligible fluctuations, due to unavoidable spontaneous emission that accompanies the stimulated emission process [14]. Phase and frequency noise could degrade the performance of coherent LADAR systems, however they do not manifest directly in incoherent detection schemes. The relative intensity noise (RIN), on the other hand, has a detrimental effect on direct detection as well. RIN is quantified in terms of the power spectral density of the intensity fluctuations, normalized to the average power. Typical InGaAsP laser diodes operating at 1.55 µm exhibit RIN of about -155dB/Hz [14]. By definition, SNR limitations due to RIN cannot be improved by raising the source power.

Speckle effects are caused by interference from a large collection of independent coherent radiators which arrive together to the photo-detector. Such interference occurs when the laser source is reflected from a rough surface. The number of photo-electrons subject to speckle phenomena can be modeled as a negative binomial random variable [25]. Speckle becomes dominant for highly coherent sources [16]. Much like the case of RIN, noise due to speckle scales with the source intensity.

Background or ambient noise in the context of LADAR system measurements constitutes any other light or signal that is collected by the detector and does not originate from the laser transmitter. For most practical scenarios, the background radiation is sunlight that falls on the area within the receiver's instantaneous field of view (FOV). The background photons collected by the sensor bear no information concerning the range to the target, but the shot noise that is associated with them contributes to the overall noise to the LADAR system measurement. As mentioned earlier, shot noise from background photons can be modeled as Poisson process, and its standard deviation is proportional to the bandwidth of the ambient light source [16]. Practical LADAR systems use optical band pass filters, designed to block all background photons at wavelengths other than that of the intended source.

1.2 Pulse Compression

The development of the modern radar theory owes large part of its foundation to the work of Woodward [26]. Woodward suggested that a wide pulse can be transmitted to achieve the energy required for detection, while at the same time the desired range resolution conditions could be achieved by modulating/coding the transmitted pulse in

order to have a bandwidth *B* greater than that of an unmodulated (uncoded) pulse of the same duration. The received echo can be processed to yield a narrow compressed shape, which depends on the bandwidth of the transmitted pulse and not on its duration [10-11, 26]. This process led to the development of a significant technological development in the design of RADAR/LADAR waveforms, which is popularly known as "*Pulse Compression Techniques*" [10, 12, 27-28]. The two significant design objectives of the high performance ranging systems, namely the high detection capability (requiring high energy content) and high range resolution (requiring short pulses/wide bandwidth) can be obtained simultaneously by the use of pulse compression techniques [12].

The pulse compression waveform has a duration-bandwidth product that is much larger than unity, in contrast with the unity duration-bandwidth product of an unmodulated pulse waveform. The duration-bandwidth product also quantifies the *compression ratio* of the process, since the temporal extent of the processed, compressed shaper is on the order of $1/B$. Typical compression ratios are in between 100 to 300, but could be as high as 10^5 [11].

A matched filtering is the process of correlating the received waveform echo with a replica of the transmitted signal. The output of the matched filter consists of the compressed pulse accompanied by residual responses at other instances (ranges), called *time* or *range sidelobes*. The sidelobes may conceal the existence of additional, weak targets. Frequency weighting of the output signals is usually employed to reduce these sidelobes. In these so-called *mismatched filtering* receivers, SNR of the main peaks is moderately compromised in exchange for more effective sidelobe suppression. Many pulse compression techniques have been investigated and reported in the literature [11, 15, 29-39].

Different types of modulations can be used for achieving the pulse compression. Two of the most significant and popular modulation schemes are *frequency modulation* and *phase modulation*. Accordingly, the existing pulse compression methods can be broadly categorized and listed as *frequency coding techniques* and *phase coding techniques*. The former includes Linear Frequency Modulation (LFM), stepped LFM, Non-linear FM (NLFM), and discrete frequency shift (time-frequency coding) waveforms. In this category, the LFM sequences can be regarded as the fundamental building blocks, which later led to the development of NLFM. The latter category includes *bi-phase* (Barker codes, compound Barker codes, M-sequences codes, MPSL codes, Golay codes etc.) [11, 30-33], and *poly-phase* codes (Frank codes, P1, P2, P3, P4 codes etc.) [11, 34-39]. Many researchers [11, 29-39, 40-43] have contributed in a significant manner for the development of different pulse compression waveforms.

In spite of their popularity and widespread applications, both the LFM and NLFM waveforms suffer from several drawbacks. The implementation of the associated digital signal processing scheme might be difficult, due to lack of high quality analog to digital converters (ADC) at the necessary high sampling rates [12]. Other significant limitations in LFM waveforms are the poor Doppler resolution and the inherent ambiguity between variations in range and in the Doppler frequency shift [12, 29]. The output of the LFM matched filter displays comparatively large range sidelobes (the first sidelobe is approximately –13.2 dB below the desired peak), which can be reduced at the cost of compromising the SNR [15]. On the other hand, NLFM waveforms are sensitive to Doppler frequency shift and are not Doppler tolerant. Further, the major limitations in implementation of NLFM are - (1) system

complexity, (2) limited development of NLFM generating devices, and (3) stringent phase control requirements [11-12].

Phase coding represents an innovative pulse compression technique, in which the effects of pulse compression are achieved by using discrete phase changes rather than frequency variations. Contributions of Barker [30], Turyn [31], Golay [32], Golomb and Scholtz [33], Friese [34], Borwein and Ferguson [35], Frank [36], Chu [37], Lewis and Kretschmer [38-39], are few of the most significant works in the area of discrete phase coded pulse compression sequences.

In phase-coded waveforms, the frequency remains constant but the phase of each subpulse is switched between certain predetermined M values at periodic intervals. That is, each pulse of length T_P can be considered as a contiguous set of N subpulses of duration $T = T_P/N$, with the phase of each subpulse chosen as either 0 or π (M = 2, bi-phase), as shown in Fig. 1.6, or from within a set of values of phases between 0 to 2π given by $2\pi/M$, M being an integer greater than 2 (poly-phase). Individual subpulses are designated as *chips* [12], *subpulses* [11] or *bits* [15]. In phase coding, the pulse compression ratio is on the order of N, the number of subpulses. The output of the matched filter is typically a narrow peak of width T (mainlobe), which is about N times stronger than the instantaneous power of the extended, received echo.

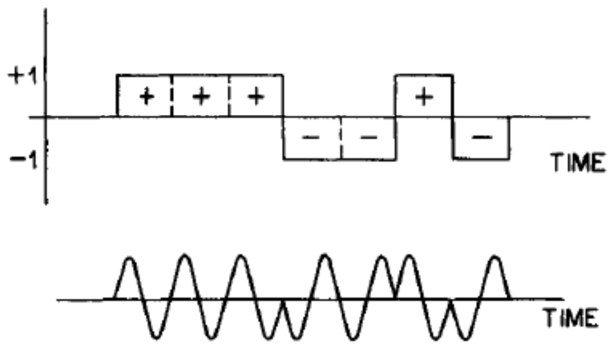

Figure 1.6 Illustration of a binary phase-coded signal. [5]

The ratio between the height of the strongest sidelobe and that of the main peak (peak to sidelobe ratio, or PSLR) of a Barker code of length N is given by $1/N$ [30]. Unfortunately, Barker codes were only found up to a length of N = 13, limiting the compression ratio accordingly. One category of longer sequences is that of maximal length pseudorandom sequences or M-sequences [10-12, 29]. However, when N is large, the PSLR of the truncated maximal length sequence approaches $1/\sqrt{N}$, which is significantly inferior to that of Barker codes. While the Barker code of length 13 produces a PSLR of –22.3 dB ($20\log(1/N)$), a 255 bits-long M-sequences is required for producing a similar ratio (sidelobe level –25.9 dB) [10].

Many searches for longer codes with optimum PSLR have been carried out [12, 29]. The resulting codes are known as *Minimum Peak Sidelobe Codes (MPSL)*, defined as binary phase codes having the best PSLR for a given length. Utilization of exhaustive search techniques resulted in MPSL codes up to a length of N = 1112 [44]. All Barker codes are also MPSL codes, but the inverse relation is not true. MPSL codes literature [12, 29, 41] reveals that the strength of the highest sidelobe is 2 for $N \leq 28$, 3 for $29 \leq N \leq 48$ and $N = 51$, and 4 for $N = 50$ and $52 \leq N \leq 70$. Recently, the MPSL code with length of N = 1112 was proposed and investigated [44]. For this code the PSL is 24 and PSLR is –33.3 dB [44].

The main advantage of bi-phase codes is their ease of implementation; however, the generation of such codes with a large number of bits requires extensive computer searches [15]. Another known class of sequences is the poly-phase codes, in which the possible phase values are not restricted to 0 or π. A number of researchers, including Friese, Frank et al., Heimiller, Chu, Lewis and Kretschmer [30-39],

investigated different types of polyphase codes and showed that they possess good autocorrelation and cross-correlation properties [15].

Friese [34] established the existence of uniform poly-phase sequences up to length 36, targeting the *Barker condition*, i.e. the magnitude of all autocorrelation sidelobes is less than or equal to one. Stochastic optimization technique was used to obtain these sequences with properly selected starting vectors. Borwein and Ferguson [35] further extended the list of known poly-phase sequences that satisfy the Barker condition, up to length 63, by using two different optimization algorithms applying stochastic and calculus techniques.

Frank *et al*. [36] established the correlation properties of the polyphase codes with M number of phases and code length N, such that $N = M^2$. These codes are popularly known as the *Frank Codes*, and it has been suggested that the Doppler shift effect of these codes can be similar to those of LFM pulse compression codes. In principle, their main limitation is that they are applied only for codes of perfect square length ($N = M^2$). Frank codes can be treated as an approximate set of stepped LFM, represented as poly-phase codes.

Lewis and Kretschmer [38-39], introduced four types of *P-Codes*, namely *P1*, *P2*, *P3* and *P4* codes, which may be treated as variants of Frank poly-phase codes. It is claimed that the *P-codes* are more tolerant to receiver band limiting prior to pulse compression than the Frank codes [11, 15, 36]. In a broad sense, it can be stated that all the Frank codes and P-codes are derived/related versions of LFM signals. The *P1* and *P2* sequences are permutations of the Frank code, and are applicable only for $N = M^2$; *P3* and *P4* codes are applicable for any length N [15]. The implementation of poly-phase coded pulses is more complex and requires extensive numerical optimization. The principal limitation of poly-phase coding is that in case

of higher sequence length, these codes become more sensitive to Doppler shift than that of the shorter ones.

1.3 Complementary Code Pairs

Another approach for sidelobe suppression is pulse compression of complementary binary sequences. A *complementary code pair*, otherwise known as a *Golay sequence pair*, is defined by the following property: a pair A_k, B_k of two L-element sequences is said to be complementary if the sum of the auto-correlations of the two sequences is zero for all nonzero shifts [32]. Thus, the sum of the autocorrelations of the two member sequences is a discrete-time delta function:

$$\sum A_{n+k} * A_n + \sum B_{n+k} * B_n = 2L\delta_k \tag{1.1}$$

$$\delta_k = \begin{cases} 1, for\ k = 0 \\ 0, otherwise \end{cases} \tag{1.2}$$

A number of iterative constructions for complementary code pairs have been derived by Golay [32]. One of these procedures, known as "appending", is applied to an L-element code pair yielding a new $2L$-element code pair [47]:

$$\left\{\frac{A}{B}\right\} \rightarrow \left\{\frac{A|B}{A|\bar{B}}\right\} \tag{1.3}$$

where $\bar{B}$ denotes the complement of B, obtained by swapping 1's and -l's, and | denotes the concatenation of sequences, e.g., $A \mid B$ is obtained by appending the elements of code B to the right of the elements of code A. Starting with the two-element Golay pair, the Golay codes of length 4 and 8 are readily derived:

$$\left\{\frac{1,\ \ 1}{1,-1}\right\} \rightarrow \left\{\frac{1,\ \ 1,\ \ 1,\ -1}{1,\ \ 1,-1,\ \ 1}\right\} \rightarrow \left\{\frac{1,\ \ 1,\ 1,\ -1,\ \ 1,\ \ 1,\ -1,\ \ 1}{1,\ \ 1,\ \ 1,\ -1,\ -1,-1,\ \ 1,\ -1}\right\} \tag{1.4}$$

This procedure may be continued on to generate sequences of lengths which are powers of two. Notice that all sequences generated this way are bipolar, with ± 1 - valued elements. In a practical application, the two sequences must be separated in time, frequency, or polarization.

In contrast to MPSL sequences, the finding of long complementary pairs is relatively simple. The generation of a new complementary pairs begins with one or two primary pairs listed in Table 1 [45], followed by the application of one of several construction rules (one of which was described above). The procedure can be repeated as needed. A recent detailed description of the presently known construction rules, including proofs, appears in section 7.3 of [45].

TABLE 1 Primitive complementary pairs

N	sequence a	sequence b
2	++	+-
10	++-+-+--++	++-+++++--
10	+++++-+--+	++--+++-+-
20	++++-+---++--++-+--+	++++-+++++---+-+-++-
26	++++-++--+-+-+--+-+++--+++	++++-++--+-+++++-+---++---

The number of possible pairs increases with length. Table 2 lists the number of known complementary pairs for all lengths up to 100 [46].

TABLE 2 Number of pairs for length $N < 100$

N	1	2	4	8	10	16	20
PAIRS	4	8	32	192	128	1536	1088
N	26	32	40	52	64	80	
PAIRS	64	15360	9728	512	184320	102912	

Note that complementary pairs are not found in all lengths. It can be shown that the possible lengths must comply with:

$$N = 2^{\alpha}10^{\beta}26^{\gamma}, \;\; \alpha, \beta, \gamma \geq 0 \tag{1.5}$$

where α, β and γ are integers. The large choice of codes, shown in Table II, helps reduce the probability of intercept (LPI) and jamming of complementary pair-encoded transmission by an adversary.

The unique autocorrelation properties of the Golay codes are shown graphically in Fig. 1.7 [47]. The upper two plots (Fig. l.7a and 1.7b) show the individual autocorrelations of each one of a 64-bit complementary code pair. The value of each of the autocorrelation peaks is equal to the number of bits in the individual code. Each of the individual autocorrelations also exhibits sidelobes that are up to 10 percent of the peak height. However, when the autocorrelations are added together, the peaks add together to a value of $2L$, whereas the sidelobes cancel out exactly.

It is this contribution of all of the bits to the autocorrelation peak, along with the complete cancellation of the sidelobes, which allows the compression of complementary code pairs to work in practice. Note that in realistic system, the computation of the correlation functions might be imperfect due to various reasons, introducing residual nonzero sidelobes.

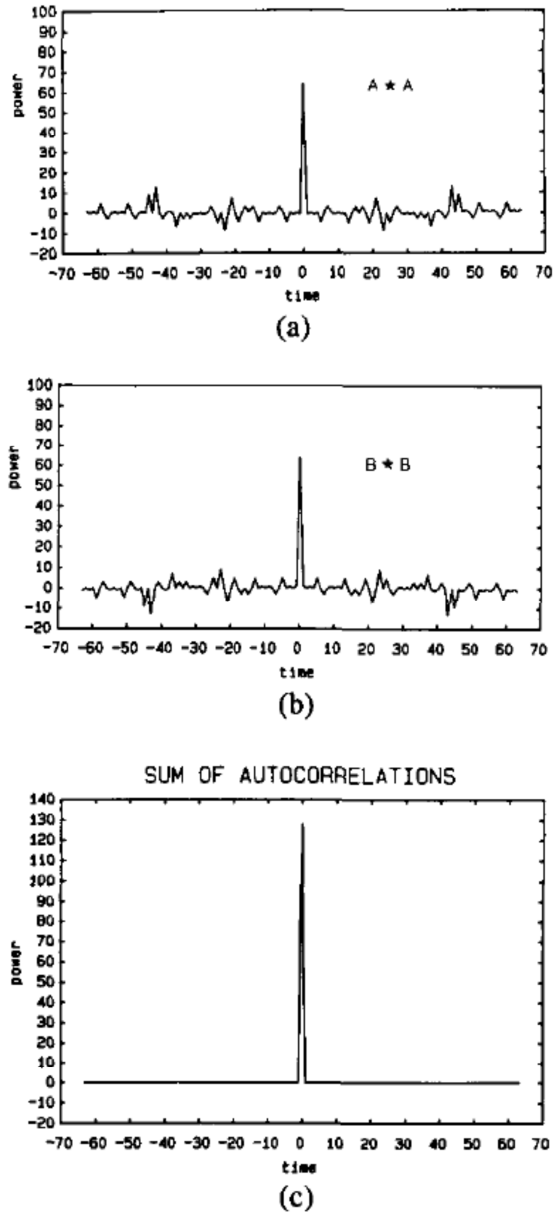

Figure 1.7 Complementary code autocorrelations: (a) and (b) are individual autocorrelations of each code of a 64-bit Golay code pair, (c) is the sum of the autocorrelations. [47]

In conventional coherent RADARs, the two sequences are usually modulated on consecutive pulses, which are then jointly and coherently processed using matched filters. The pulse repetition interval (PRI) needs to be large enough to avoid range ambiguity. The main drawback in RADAR use of complementary code pairs is the sensitivity to Doppler shift. If during the PRI the range to the target has changed by a

meaningful fraction of the wavelength, the second pulse will exhibit an additional phase shift that will degrade or destroy the complementarity property of the pair. Direct-detection laser applications of complementary pair coding are insensitive to phase. However, straight-forward direct detection of the code pair would remove all phase information, and inhibit the compression of the pulses altogether. As will be discussed in detail later in subsequent sections, the complementary phase codes can be brought into an analogous unipolar (AM) representation, which nearly retains the sidelobe suppression qualities of the original pair, following simple direct detection. Therefore, the use of AM versions of complementary pairs in LADAR applications is immune to the main drawback of the original phase codes.

1.4 LADAR System Based on Incoherent Pulse Compression

The straight-forward application of phase codes to a LADAR system would require a coherent receiver, which comes at the cost of significant complexity [14]. Recently, a new approach for the compression of incoherently detected pulse sequences was introduced by Prof. Nadav Levanon from Tel-Aviv University [48]. The phase changes of a chosen bipolar phase code are translated to a pulse position modulation through a process called Manchester coding, which will be introduced in detail in Chapter 2. The encoding process results in a binary, intensity modulated sequence, hence reflected echoes can be received by simple incoherent detection. Nevertheless, the post-detection processing algorithm proposed in [48] yields PSLR and performance which nearly replicates that of the original bipolar phase code. With the exception of two time slots immediately adjacent to the main lobe, the PSLR of

the incoherently compressed code pair is $1/2L$. For example, the compressed form of a pair of 416 elements-long sequences yield a theoretical PSLR of -58.4 dB.

The cross-correlation sidelobes are further reduced by using a longer reference seqeunce [48, 52], based on Manchester coding of a mismatched filter designed for the original binary code. The penalties associated with such a filter are a modest loss to the main peak power, on the order of only 1 dB, and the processing of an analog-like, multilevel reference sequence instead of a binary one. The method provides considerable relaxation in the LADAR receiver architecture, compared with the coherent setup that would normally be necessary for the processing of the bipolar phase sequence, while retaining most of the performance benefits of using that sequence.

Natural candidates for the incoherent pulse compression procedure are binary phase codes. In this thesis, MPSL codes of 82 and 1112 bits length, as well as complementary pair codes of 416 and 832 bits length, are being used. With incoherent compression of these codes, laser ranging was demonstrated at poor SNR conditions, as low as -20 dB [44]. The noise tolerance can be leveraged towards a longer measurement range, lower launch power and energy consumption, reduced apertures and improved operation at unfavorable atmospheric conditions.

1.5 Signal-to-Noise Improvement When Using Complementary Code Pairs

Ideally, and ignoring sidelobes for a moment, the strength of the main lobe obtained following the compression of an L-element sequence is a factor of L better

than that of a single sub-pulse of equal intensity and duration. However, the outcome of the correlation in a real-world system is always degraded by noise of various sources. Let us assume that the noise waveforms add to different samples of the coded signal are statistically uncorrelated to one another. When the signal is bipolar with ±l values, the correlation reduces to signed addition of L samples, thus the noise contributions add on a root mean squared basis, i.e., noise builds up by a factor of $\sqrt{\mathrm{L}}$. The overall SNR improvement with respect to a single sub-pulse is therefore [47]:

$$\frac{L}{\sqrt{L}} = \sqrt{L} \tag{1.6}$$

In the case of the complementary bipolar code pair, the reconstructed response is $2L$ times larger than that if a single sub-pulse. However the noise propagated through the system also increases by a factor of $\sqrt{2\mathrm{L}}$ (it builds up by a factor of $\sqrt{\mathrm{L}}$ for each correlation and by a factor of $\sqrt{2}$ when the two correlation results are added [47]). The net overall improvement in SNR following the addition of the two auto-correlations is then:

$$\frac{2L}{\sqrt{2L}} = \sqrt{2L} \tag{1.7}$$

In an incoherent pulse compression laser ranging systems, the on-off keying of optical power only provides unipolar (nonnegative) signals, curtailing direct transmission of bipolar content. Since energy is only transmitted during half of the code symbols, the SNR is degraded by a factor of $\sqrt{2}$. The overall SNR improvement with respect to a single sub-pulse is therefore given by:

$$\frac{\sqrt{2L}}{\sqrt{2}} = \sqrt{L} \tag{1.8}$$

An averaging process over repeating acquisitions of the received signal will improve the SNR by a factor of $\sqrt{N}$, where N is a number of averages over repeating transmissions of the same sequence. Thus, the system SNR can be improved by a factor of $\sqrt{NL}$, if both pulse compression and averaging are applied.

1.6 Use of Phase Codes in Fiber-Optic Signal Processing

A method of optical time domain reflectometry (OTDR), proposed in the late '80s by Moshe Nazarathy et al. [47], first realized the advantage of using pairs of probe signals that have complementary autocorrelation properties. Since OTDR equipment makes use of square-law detection, there is no way to probe the fiber with negative signals, therefore the authors proposed a correlation technique that employs unipolar signal processing based on Golay codes. The results demonstrated an improved dynamic range, reduced measurement time, SNR improvement without compromising resolution, and strong sidelobe suppression.

Another demonstration of fiber-optic signal processing based on Golay codes was proposed and demonstrated by Marcelo Soto *et al*., in the context of distributed Brillouin fiber sensors [50]. Positive-valued elements of the code were represented as Brillouin gain, whereas negative-valued elements were replaced by Brillouin loss. The positive and negative elements were transmitted as pulses of the lower and upper frequency sidebands of a modulated Brillouin probe wave, respectively. The proposed scheme allowed for fiber sensing over 50 km with 2 m spatial resolution. The use of bipolar Golay sequences provided a higher SNR enhancement and stronger robustness

to pump depletion in comparison to Brillouin optical time domain analysis (BOTDA) systems employing conventional unipolar sequences.

Lastly, Yair Antman *et al*. also demonstrated the added value of advanced RADAR-based phase-coding techniques in the distributed Brillouin fiber sensors and signal processing [51]. The off-peak reflectivity of dynamic Brillouin gratings (DBGs) over polarization maintaining fibers was reduced considerably through the encoding to the writing pump beams by so-called 'perfect Golomb codes'. The cyclic auto-correlation function of these binary phase codes assumes zero off-peak values. Golomb-coded DBGs allowed for longer variable delay of one-time probe waveforms with higher SNRs and without averaging [51].

1.7 Research Objective

The primary objectives of this dissertation are to propose, analyze, simulate and demonstrate a better trade-off between range and resolution in simple, direct-detection LADAR systems, using the incoherent compression of complementary Golay code pairs. The outcome of the research program could enable new and innovative LADAR configurations having a potential for lower probability of intercept, reduced power consumption, smaller apertures, and better performance at unfavorable atmospheric conditions.

CHAPTER

2

LADAR with incoherent pulse compression

2.1. Incoherent pulse compression for laser ranging and detection

This chapter deals with a compression of an incoherently detected unipolar pulse sequences, and its application to a short range laser range-finder system. The compression principle relies on a unipolar representation of known bipolar phase codes, such as MPSL sequences and complementary Golay codes. After introducing the underlying principle and a link budget calculation, simulations of the incoherent compression of unipolar derivatives of MPSL codes, 82 bits and 1112 bits in length, as well as complementary pair codes, 416 bits and 832 bits in length, are reported. Simulations are carried out for different SNR levels. Next, the incoherent compression of the 1112 bits-long MPSL sequence and the 832 bits-long complementary pair are demonstrated experimentally, using a simple optical link: the sequences are used to drive an electro-optic amplitude modulator, and they are recovered through simple direct detection. The sidelobes of the compressed waveform are suppressed by as much as 46 dB and 42 dB for MPSL and complementary codes respectively, with respect to the main correlation peak power. Lastly, the principle is

used in a laser range-finder setup demonstration. A depth resolution of 3 cm was demonstrated.

2.2. Correlation domain analysis, match-filtering and side lobe suppression

At the LADAR receiver, the returning echoes $s(t)$ are cross-correlated with a replica of the launched waveform $h(t)$ to obtain an impulse response:

$$S_0(\tau) = s(t) \otimes h(t) = \int_{-\infty}^{\infty} s(t)h(\tau - t)dt \quad (2.1)$$

The cross-correlation produces a peak at a delay τ which corresponds to the round-trip propagation time from the source to the target and back to the processing unit. Any off-peak residual correlation manifests as background noise in the LADAR trace. Use of the launched waveform itself as reference, known as matched filtering, is known to maximize the ratio of intended peak strength to that of the background in the presence of additive white Gaussian noise in the channel [15]. The temporal width of the correlation peak determines the spatial resolution of the laser ranging system. The resolution is quantified as the full width at half maximum of the correlation main lobe (see Fig. 2.1).

As discussed in the introduction with respect to sequence coding schemes, the reduction of correlation sidelobes is critical to the detection of weak, multiple targets. The sidelobe strength is sensitive to the specifics of the waveform being used. The sidelobe suppression performance of a ranging system is quantified in terms of two primary figures of merit: the PSLR already discussed, and the integrated-sidelobe-ratio (ISLR) (see Fig. 2.1). The PSLR is the ratio of power levels between the main

lobe peak and the highest sidelobe peak, and it determines the performance of the system in the presence of a point interfering disturbance. The ISLR is the ratio of the energy within the main lobe to the energy outside the main lobe (illustrated in Fig. 2.1 as the ratio between the red painted area and the yellow painted area), and it determines performance in the presence of distributed interference. Resolution is defined as the full width at half maximum (FWHM) of the main correlation lobe. The intersection of the impulse response with the -3 dB line (dashed), defines the boundaries of the mainlobe for all the above.

In various LADAR applications further suppression of the sidelobes is necessary, in order to improve the dynamic range and contrast. The correlation sidelobes can be suppressed by applying an amplitude weighting function to the waveform [53] or by using sophisticated compression codes with the high sidelobe suppression ratios, as was discussed in the Chapter 1.

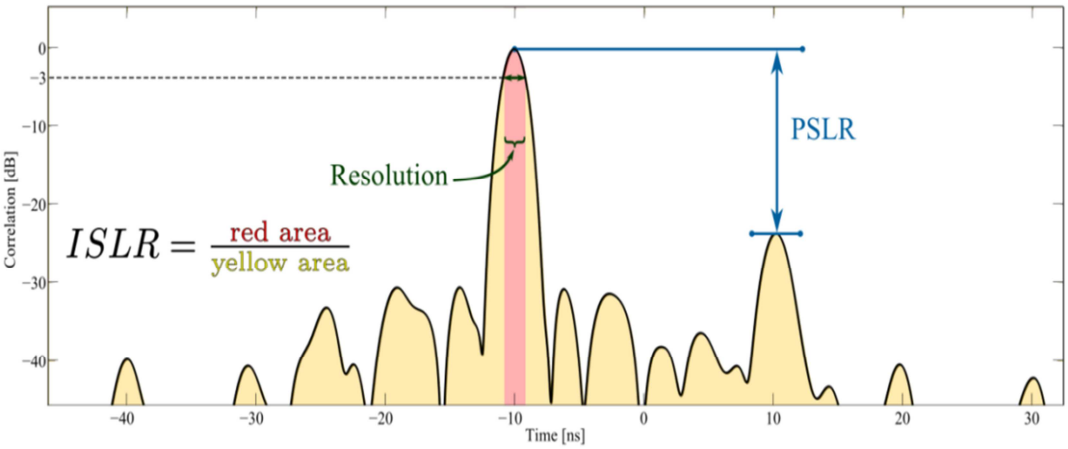

Figure 2.1 Definitions of PSLR, ISLR and resolution. [54]

2.3. LADAR Link Budget

In this section, the expected range and resolution of the LADAR system used in this work are estimated, taking into consideration the noise of its various

constituent components. A NIST report defines resolution as “the smallest distance separation between two distinct objects illuminated by a LADAR source that can be detected in the signal return.” [55]. As discussed earlier, the spatial resolution of the system is inversely proportional to the operating bandwidth [15]:

$$D = \frac{c}{2 \cdot B} \tag{2.2}$$

Where c is the speed of light in vacuum and B is the total bandwidth of the transmitting source. The light source used in our experiments is modulated by waveforms of 1 GHz bandwidth that corresponds to a spatial resolution of about 15 cm.

The *ranging accuracy* is defined as the absolute error in the range measurement. Unlike resolution, it is also related to SNR considerations, according to [28] (see Fig. 2.2):

$$\sigma_R = \frac{c}{2 \cdot B \cdot \sqrt{2 \cdot SNR}} \tag{2. 3}$$

For example, a signal source of 1 GHz bandwidth at a SNR of 20 dB yields ranging accuracy of about 1 cm.

In order to estimate the optical signal to noise ratio (OSNR) and the electrical signal to noise ratio (ESNR), the noise contributions of various mechanisms need to be evaluated (see Chapter I for the introduction of the noise mechanisms). Noise contributions in the electrical and RF parts of the system include the electronic noise of the RF amplifier, and the sampling error of the digitizing oscilloscope. The contribution of the RF amplifier is quantified in terms of its noise figure (or NF), and equals to 7 dB in our case. The noise figure represents the degradation in the ESNR going through the amplifier. The amplifier was not used in all measurements.

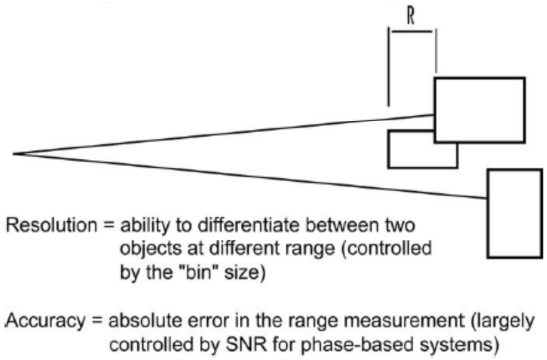

Figure 2.2 Range accuracy versus resolution. [16]

The noise floor of the oscilloscope, while operated at maximum sensitivity, is on the order of 0.2 mV_{RMS}. The optical-to-electrical conversion factor of the amplified photo-detector that we used is 40kV/W. Hence, the oscilloscope uncertainty is equivalent to an error of about 5 nW (-53 dBm) in the measurement of optical power. As seen next, this source of noise is dominated by other mechanisms.

Noise in the electro-optical parts of the setup consists of the photo-detector thermal noise, amplified spontaneous emission of optical amplifiers, and intensity noise of the distributed feedback (DFB) laser diode source of our LADAR system. Detector thermal noise is often quantified in terms of its noise-equivalent power or NEP (see section 1.1.5. for more details):

$$P_{PD} = NEP \cdot \sqrt{B} \tag{2.4}$$

Here P_{PD} represents the optical power at the detector input, for which an ESNR of unity is expected at the detector output. It is assumed here that the integration bandwidth of the detector circuitry matches the bandwidth of the optical waveform.

For the lab experiments I used an avalanche photodiode detector (APD), a device that is widely used in LADAR systems. It is essentially a detector that

possesses inherent electrical gain. Within a conventional PIN photodetector, a photon striking the detector surface has some probability of producing a single photoelectron, which in turn produces a current within the detector circuit that can be converted to a voltage. The APD is a detector that produces a flood or avalanche of photoelectrons from a single incoming photon. The gain of the APD (M-factor) dictates how many electrons are produced by each photon that is successfully converted into a useful signal. The quantum efficiency of the detector determines the probability of causing the avalanche. The APD detector used in the experiment is characterized by an ESNR of unity at P_{PD} of -43 dBm (50 nW) at 1550 nm wavelength at 1GHz bandwidth, and has an optimal performance at an M-factor 10. The NEP value includes excess noise due to the uncertainty in the amplification factor M, which is on the order of 3.5dB. Compared with a PIN photo-diode of equal bandwidth and thermal noise, the APD provide an improvement of 6.5 dB in ESNR.

The variations in optical power due to RIN of the laser diode source are given by:

$$P_{RIN} = \sqrt{10^{RIN/10} \cdot B} \cdot P_{CW} \tag{2.5}$$

where RIN expresses the power spectral density of the source intensity noise, which is assumed to be constant across the bandwidth of interest. RIN is typically on the order of -155 dB/Hz in InGaAsP laser diodes operating at 1.55 µm. P_{CW} represents the operating CW optical power. Equation (2.5) suggests that the optical power that is equivalent to RIN-induced noise, at a bandwidth of 1 GHz, is -32.5 dB below the average optical power of the collected signal. The collected optical power levels at our laser range finder experiments are typically very low, on the order of -50 dBm. Therefore, RIN-induced noise is negligible.

The erbium-doped fiber amplifier (EDFA) used in our experiments amplifies the transmitted signal power at the laser diode output by a gain G of 25 dB, up to Pt = 25dBm. Photo-current noise in the detection of amplified signals stems from both the interference between signal and ASE (known as 'signal-spontaneous interference'), and the detection of ASE power itself (sometimes referred to as 'spontaneous-to-spontaneous interference') [14]. ASE spans the entire gain bandwidth of the EDFA, which is on the order of 4 THz. However, an optical bandpass filter is used to restrict the bandwidth of ASE that reaches the detector to several GHz, on the order B. In this condition, the dominant EDFA-induced noise term stems from the interference between the desired signal and those ASE components that fall within the optical filter passband. The ESNR of the photo-current following the detection of the amplified signal would be:

$$P_{CW}/(2 \cdot h\nu \cdot NF \cdot G \cdot B) \tag{2.6}$$

Here the noise figure NF of EDFAs is on the order of 3 (5 dB), and $h\nu$ = 1.28e-19 [J] is the energy of a photon at 1550 nm wavelength. Assuming P_{CW} of 1 mW (0 dBm) at the laser diode output, the ESNR is over 1,000 (30 dB). In similarity to the preceding discussion of RIN, noise due to optical amplification can be neglected with respect to thermal noise. In summary, we conclude that the system ESNR would be dominated by thermal and multiplication noise in the APD receiver, and by noise of RF amplifiers (when used).

With the noise of the detection setup established, we evaluate next the expected optical power that is reflected from at target and is incident upon the receiver. The optical power of the collected echoes P_r at the input of the photo-detector is given by the LADAR range equation [16]:

$$P_r = \frac{D_R^2 \cdot \rho_t \cdot dA \cdot P_t}{R^2 \cdot \theta_R \cdot (\theta_t \cdot R)^2} \tag{2.7}$$

Here D_R is the diameter of the circular receiver aperture, and ρ_t is the target reflectance parameter. Typical values for this parameter range from as little as 2% to as high as 25% at long wavelengths. The reflectance of white walls used in most experiments was estimated as ρ_t = 7%. dA is the target surface area, θ_t is the laser beam angular divergence angle, θ_R is the angular dispersion of light reflected from the target surface, and R is the one-way distance to the target. The beam divergence θ_t is given by the diffraction limit [16]:

$$\theta_t = \frac{1.22 \cdot \lambda}{D_t} \tag{2.8}$$

In our experiments, the wavelength was λ = 1550 nm and the transmission aperture diameter was $D_t = 10$ cm, leading to an angular beam divergence of 0.02 mrad. In these conditions the illuminating beam in the target plane is smaller than the target surface area, and dA simply becomes the projected area of the beam at the target:

$$dA = \frac{\pi \cdot \theta_t^2 \cdot R^2}{4} \tag{2.9}$$

For a Lambertian reflecting target, such as those used in our experiments, the solid angle θ_R over which reflected radiation is dispersed takes the value of π steradians. Substituting the above parameters into the LADAR receiver budget range equation (2.7), the following simple expression is obtained:

$$P_r = \frac{D_R^2 \cdot \rho_t}{4 \cdot R^2} P_t \tag{2.10}$$

Simulations and experiments of compressed sequences suggest that the lowest ESNR in which the correlation peak of an incoherently-compressed, 1000 bits-long

sequence could still be observed is about -20 dB. Therefore, the longest measurement distance is that for which the incoming signal power P_r is 10 dB below the NEP of the photo-detector. This minimal received power is therefore estimated to be on the order of -53 dBm. Assuming a transmitted power of 25 dBm and the receiver circular aperture of 10 cm, the signal power would drop to that limiting level for R of about 100 m. The working distance can be further increased with averaging as was discussed in section 1.5. The OSNR (in dB) in which the main correlation peak remains discernible is improved by a factor of $\sqrt{N}$, where N is the number of independent recordings to be averaged.

2.4. Coding principle

The primary motivation for incoherent pulse compression is to try and obtain the sidelobe suppression performance that can be provided by phase-coded pulse sequences, while employing simple direct detection technique that is fundamentally phase-insensitive. The principle is of particular consequence in LADAR schemes, since it eliminates the need for complicated optical coherent receiver.

2.4.1 Coding procedure

Consider a bipolar code of length N: $c[n]$, such as an MPSL sequence or other (see Chapter 1 for the discussion of different phase-coded pulses sequences), where $n = 1..N$. A unipolar code of length $2N$ is generated based on $c[n]$ by applying Manchester coding: if $c[n] = 1$, then $T[2n-1] = 1$ and $T[2n] = 0$. For $c[n] = -1$, $T[2n-1] = 0$ and $T[2n] = 1$ are chosen instead [48]. Manchester coding converts the bipolar phase information into pulse-position modulation, and it is

used in optical communication [56]. The code T would later be used in intensity modulation of the LADAR light source.

A bipolar matched filtering sequence R of length $2N$ is constructed in a similar manner: $R[k]$ is set to 1 if $T[k] = 1$ and equals -1 if $T[k] = 0$, $k = 1..2N$ [48]. The code R is digitally stored at the receiver for post-detection processing. Using a matched bipolar reference signal instead of a unipolar signal results in a cross-correlation (between T and R) with an average value of zero. Since the sequence R is used only digitally, its bipolar nature does not overburden the LADAR setup.

As an example, the construction of T and R codes corresponding to the Barker 13 bipolar sequence is illustrated in Fig. 2.3. The transmitted signal (top) is a dense batch of narrow pulses. In the absence of noise, directly detected reflections from targets would be scaled and delayed replicas of the transmitted signal. The reference signal (bottom) is a dense batch of bipolar pulses, stored numerically in the receiver. The aperiodic cross-correlation between these two codes is shown in Fig. 2.4 (bottom), alongside the aperiodic auto-correlation of the original Barker 13 sequence itself (top). With the exception of the two sidelobes immediately adjacent to the main correlation peak, the cross-correlation replicates the sidelobe suppression of the original bipolar code [48]. In contrast, the auto-correlation of a unipolar representation $\tilde{c}[n]$ of the Barker code itself, in which -1 symbols are simply replaced by 0, exhibits inferior sidelobe suppression performance (Fig. 2.4, center).

The cross-correlation sidelobes can be further suppressed using a mismatched filtering process, in which the sequence R is replaced by a longer code $\tilde{R}$, whose coefficients are not restricted to ±1. Substantial sidelobe suppression can be obtained, at the cost of a modest degradation in the central correlation peak power [15]. The

sequence $\tilde{R}$ can be designed to maximize the ISLR, according to principles described in sec. 6.6 of [15].

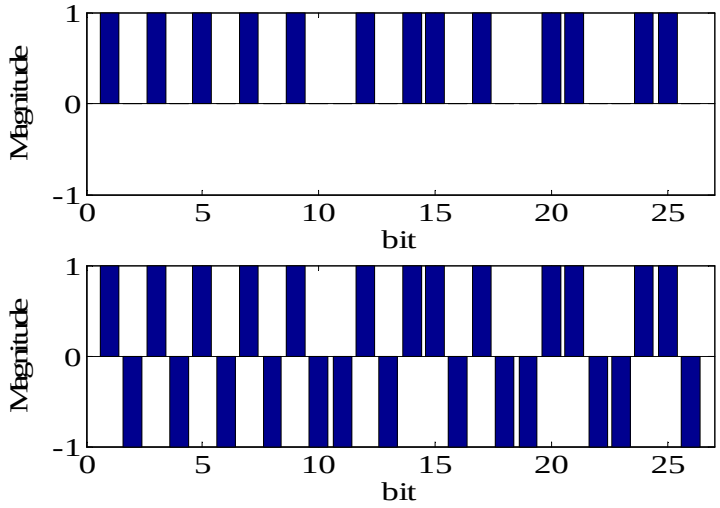

Figure 2.3 Transmitted code *T* (top) and matched filtering code *R* (bottom) corresponding to the Barker 13 code: [+1 +1 +1 +1 +1 -1 -1 +1 +1 -1 +1 -1 +1].

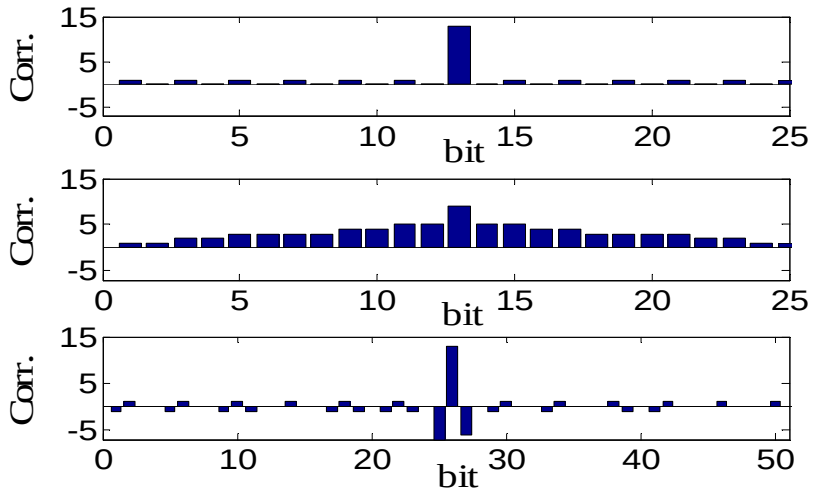

Figure 2.4 Top – aperiodic auto-correlation of the Barker 13 bipolar code: [+++++--++-+-+]. The correlation peak is 13, whereas the maximal sidelobe equals unity. Center – aperiodic auto-correlation of a unipolar representation of the Barker 13 code: [1111100110101], showing a weaker central peak and inferior sidelobe suppression. Bottom – aperiodic cross-correlation between the transmitted code *T* and matched filtering code *R* corresponding to the Barker 13 bipolar code (see Fig. 2.3). With the exception of the two time slots in the immediate vicinity of the central peak, the suppression of sidelobes reaches that of the original bipolar sequence [44].

In coherent receivers, negative sidelobes (such as in Fig. 2.4. bottom) can cause two problems [48]: 1) they could mask-out the main lobe of a nearby weaker

target; and 2) due to possible phase change of the carrier frequency of the reflected signal, negative sidelobes can change their sign. Together with measurement noise, the negative sidelobes could lead to false alarms or miss-detections. In incoherent receivers, the current that is directly provided by a photo-detector is phase insensitive, so problem 2 in unlikely to happen.

The strong negative sidelobes can still mask a weaker target, but only if the delay difference between the two targets matches the duration of a single code bit. For a relatively wide reflection targets, the negative sidelobes can be differentiated, emphasizing edges while still maintaining the system resolution [48]. Without loss of generality, the two negative sidelobes immediately adjacent to the main correlation peak will be neglected for the rest of this chapter.

2.5. Simulated sidelobe suppression

In order to evaluate the proposed method for incoherent pulse compression, its performance was simulated for two Manchester-coded MPSLs that are 82 and 1112 bits long, respectively, and two complementary pair codes that are 416 and 832 bits long, respectively. The MPSL and complementary pair codes themselves are provided in Appendix A.

2.5.1. MPSL 82

First, 82 bits-long MPSL code was used. The transmitted, Manchester coded sequence T is illustrated in Fig. 2.5 (top), alongside its matched reference R (center). The noise-free aperiodic cross-correlation between these two codes is shown in Fig. 2.5 (bottom), with a PSLR of 26.24 dB. The miss-matched reference $\widetilde{R}$, specially

designed for the sequence T, is illustrated in Fig. 2.6 (center), alongside the noise free aperiodic cross-correlation between T and $\widetilde{R}$. Note that the sequence $\widetilde{R}$ is three time longer than R, and that its values are not restricted to ±1. The PSLR is improved by 8 dB, while the main lobe power is attenuated by 0.9 dB (Fig. 2.6, bottom).

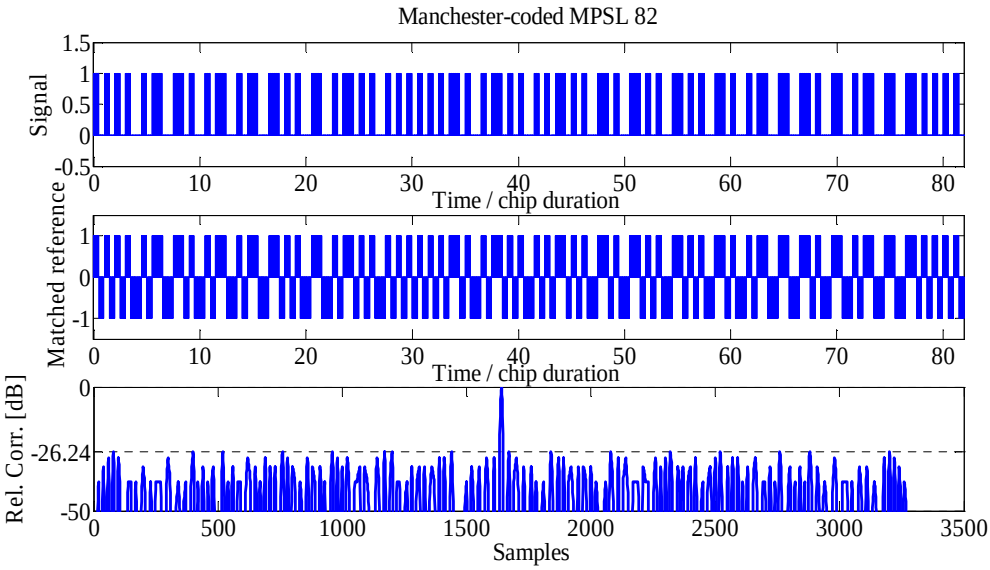

Figure 2.5 Transmitted code T (top) and matched filtering code R (center), corresponding to the MPSL 82 code. Bottom – aperiodic cross-correlation between the transmitted code T and matched filtering code R.

Next, additive Gaussian-distributed noise was introduced to the simulation. The incoherently compressed forms of the 82 bits-long MPSL sequence are shown in Fig. 2.7, for different SNR values and for both matched and mismatched filtering. At a high SNR of 20 dB, the PSLR of the match-filtered sequence was 26 dB, and a mismatched filter further improved the PSLR to 32 dB, with a 1 dB attenuation of the main lobe (Fig. 2.7, top row). When the noise and signal power levels are equal (center row), the simulated PSLR was 16.4 dB, and the sidelobe suppressions obtained with matched and mismatched filters were practically equal. At a negative SNR of -5 dB (bottom row), the main correlation peak still can be recovered at a PSLR of about 6.7 dB. Here too, the mismatched filter gave no benefit in the sidelobe suppression. Sidelobe suppression was further tested in an extremely noisy condition,

at which the applied noise power was 100 times larger than that of the signal (Fig. 2.8). In this scenario, the main correlation peak can no longer be recovered.

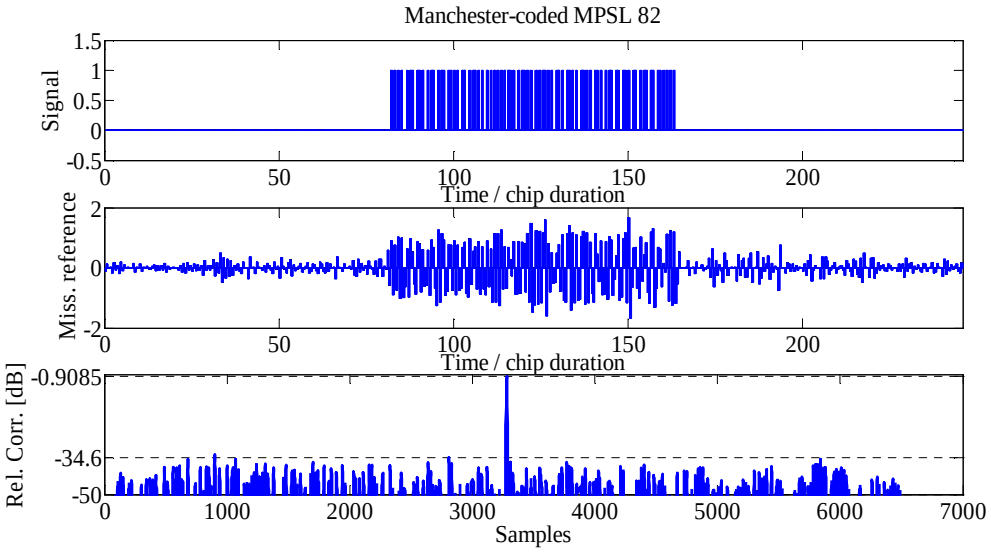

Figure 2.6 Transmitted code T (top) and miss-matched filtering code $\tilde{R}$ (center), corresponding to the MPSL 82 code. Bottom – aperiodic cross-correlation between the transmitted code T and matched filtering code $\tilde{R}$.

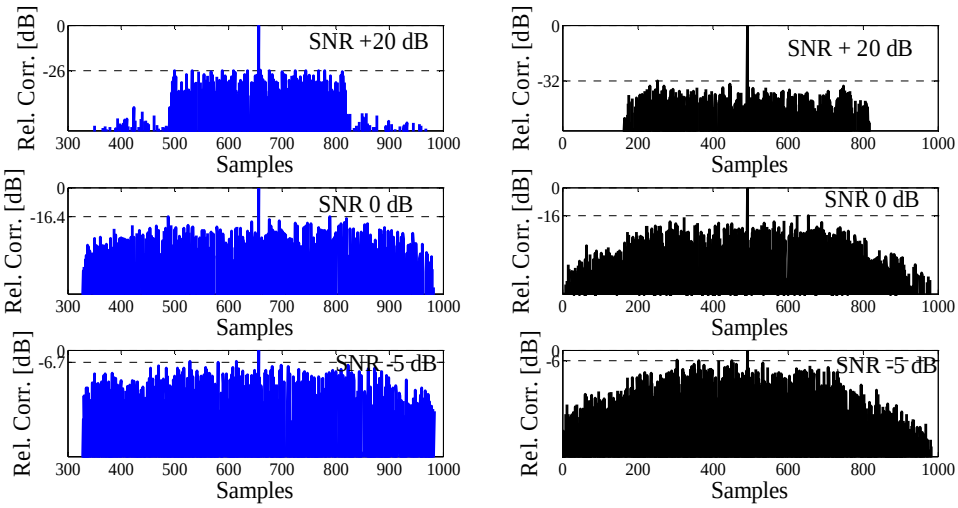

Figure 2.7 Cross-correlations of incoherently compressed, 82 pulses-long unipolar sequences. Both matched (left, blue) as well as mismatched (right, black) filters were used in the compression process. Top row: simulated compression with a signal-to-noise ratio of +20 dB. Center row: simulated compression with a signal-to-noise ratio of 0 dB. Bottom row: simulated compression with a signal-to-noise ratio of -5 dB.

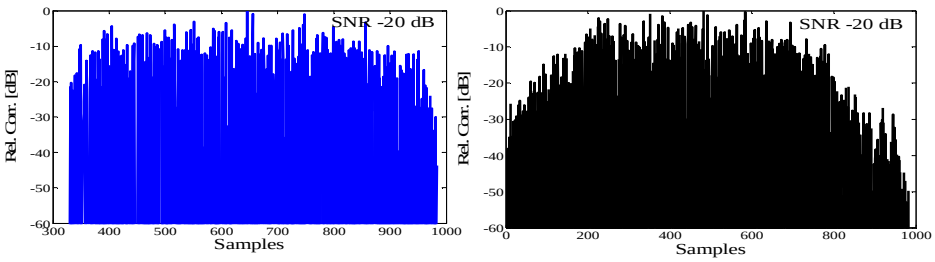

Figure 2.8 Cross-correlations of an incoherently compressed, 82 pulses-long unipolar sequence with a signal-to-noise ratio of -20 dB. Both matched (left, blue) as well as mismatched (right, black) filters were used in the compression process.

2.5.2. MPSL 1112

Similar simulations were also carried out for a 1112 bits-long MPSL code. The transmitted Manchester coded sequence T is illustrated in Fig. 2.9 (top), alongside its matched reference R (center). The noise-free aperiodic cross-correlation between R and T is illustrated in Fig. 2.9 (bottom) with a PSLR of 33.3 dB.

Here too, the sidelobes can be further suppressed using a specially designed mismatched sequence $\widetilde{R}$ (Fig 2.10 center). The noise-free aperiodic cross-correlation between $\widetilde{R}$ and T is illustrated in Fig. 2.10 (bottom). The PSLR in this case equals 51.6 dB, with a 0.9dB attenuation to the main lobe.

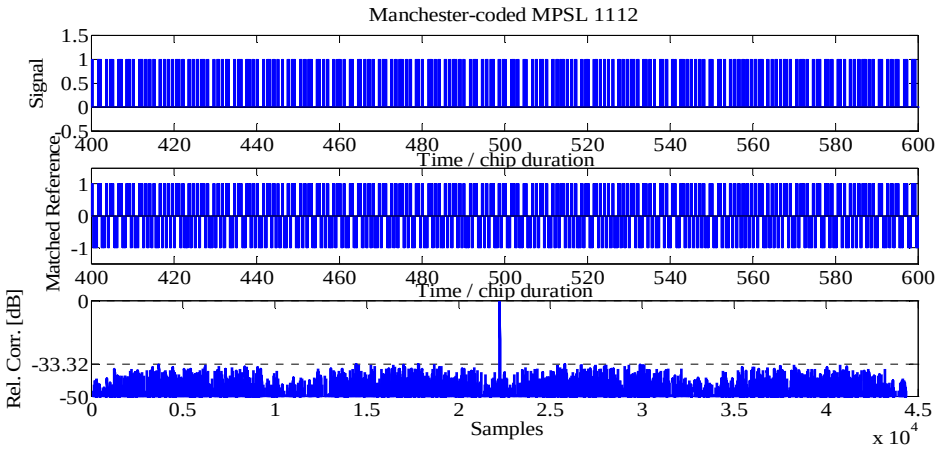

Figure 2.9 Transmitted code T (top) and matched filtering code R (center), corresponding to the MPSL 1112 code. Bottom – aperiodic cross-correlation between the transmitted code T and matched filtering code R.

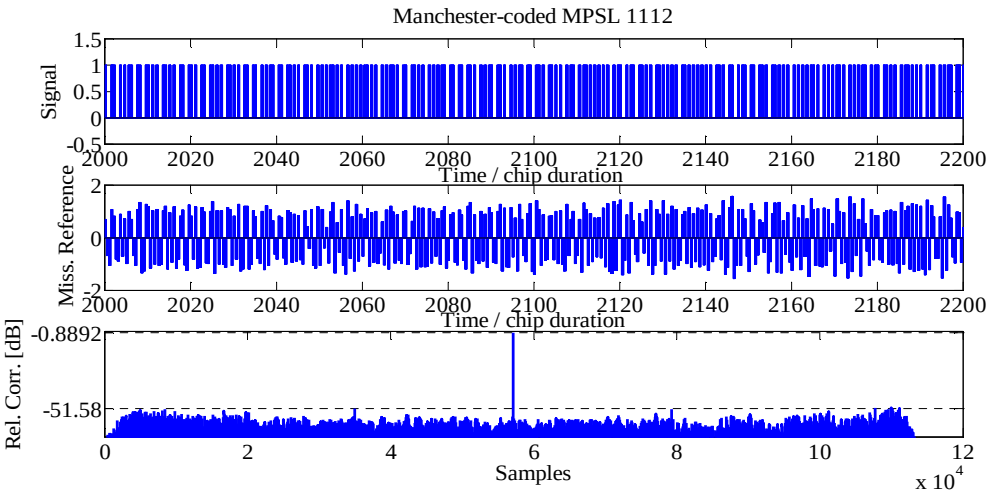

Figure 2.10 Transmitted code T (top) and miss-matched filtering code (center) corresponding to the $\tilde{R}$ (center), MPSL 1112 code. Bottom – aperiodic cross-correlation between the transmitted code T and miss-matched filtering code $\tilde{R}$.

Sidelobe suppression at +20 dB, 0 dB, and -20 dB SNR levels are illustrated in Fig. 2.11. At a high SNR of +20 dB, the PSLR of the matched filtered sequence reached 31.8 dB (top row), and a mismatched filter further improved the PSLR to 43 dB with 1 dB attenuation of the mainlobe. At an SNR level of 0 dB, the PSLR for matched and mismatched filtering reached 25.2 dB and 24.6 dB respectively, with a miss-match-induced loss of 1 dB to the mainlobe. This time, long length of the sequence allowed for a recovery of the main lobe even at poor SNR levels as low as -20 dB, with a PSLR of approximately 9 dB in both cases. As mentioned before, mismatch filters provide no added value for SNR levels below 0 dB.

While the using of MPSL code brings together the simplicity of incoherent direct detection and the sidelobe suppression, the scaling of the obtained performance is rather difficult. The further suppression of the sidelobes may be pursued in one of two manners: first, since the PSLR scales with the length of the MPSL sequence, longer codes may be used. However, the search for such codes is a daunting task.

Alternatively, the incoherent compression of complementary code pairs, whose length can be scaled arbitrarily following simple design rules, is presented next.

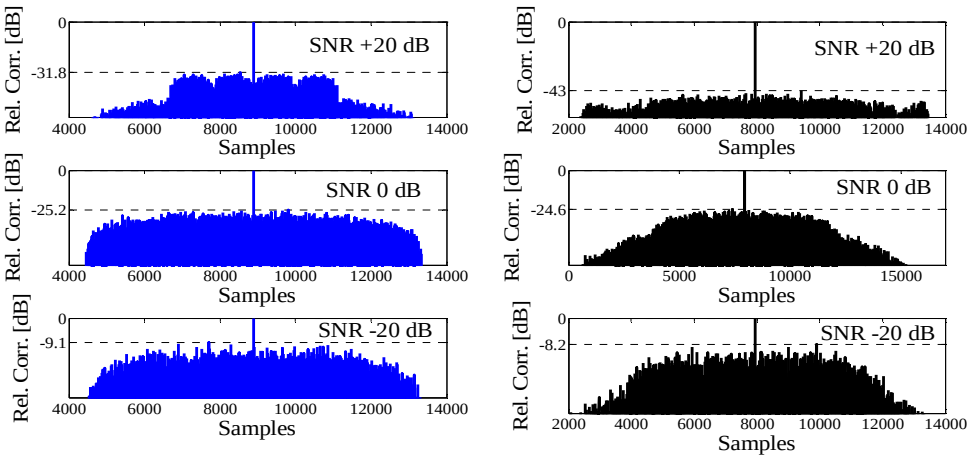

Figure 2.11 Cross-correlations of an incoherently compressed, 1112 pulses-long unipolar sequence. Both matched (left, blue) as well as mismatched (right, black) filters were used in the compression process. Top row: simulated compression with a signal-to-noise ratio of +20 dB. Center row: simulated compression with a signal-to-noise ratio of 0 dB. Bottom row: simulated compression with a signal-to-noise ratio of -20 dB.

2.5.3. 416 bits-long complementary pair

This time, 416 bits-long complementary pair codes were simulated. The pair of complimentary codes is characterized by the following useful property: the auto-correlation sidelobes of one code are equal in magnitude to those of the other code, albeit with an opposite sign [14]. Adding the matched-filtered forms of the two codes together, therefore, reduces the sidelobe power drastically [15]. The advantage of using complementary code pairs is two-fold: 1) unlike MPSL sequences, their length is scalable through several simple procedures [16], some of which were described in previous sections; and 2) the obtained sidelobe suppression is equivalent to, or better than, that of a mismatched-filtered MPSL sequence of similar length.

The generation of a new complementary pair starts with one or two of the primitive pairs listed in Table I (Section 1.3, Chapter 1), followed by the application

of one of several construction rules. The procedure can be repeated as needed. A recent detailed description of the presently known construction rules, including proofs, appears in section 7.3 of [45]. The most basic construction rule [32], which creates the pair {**c**, **d**} based on a pair {**a**, **b**}, is:

$$\{\boldsymbol{c}, \boldsymbol{d}\} = \{cat(\boldsymbol{a}, \boldsymbol{b}), cat(\boldsymbol{a}, -\boldsymbol{b})\} \tag{2.11}$$

where cat (**a**, **b**) stands for concatenation of the two sequences **a** and **b**. The expression **-b** implies polarity reversal of the elements of sequence **b**. This basic construction rule increases the length of the sequences in the new pair. The same rule can be used to create a different pair from the same original pair:

$$\{\boldsymbol{e}, \boldsymbol{f}\} = \{cat(\boldsymbol{b}, \boldsymbol{a}), cat(\boldsymbol{b}, -\boldsymbol{a})\} \tag{2.12}$$

The 416 bits-long code pair was generated by applying the above rule to the 26 element primitive pair of Table I (Section 1.3, Chapter 1), 4 times in succession. The transmitted Manchester coded sequence T is illustrated in Fig. 2.12 (top), alongside its matched reference R (center). The noise-free aperiodic cross-correlation between R and T is illustrated in Fig. 2.12 (bottom) with a PSLR of -58.4 dB. The ideal zero-sidelobes correlation property of the complementary pair is nearly preserved by the Manchester encoding, with a PSLR of $1/2N$, where N is the length of the each code in the pair [57].

Sidelobe suppression at +20 dB, 0 dB, and -20 dB SNR levels are illustrated in Fig. 2.13. At a high SNR of +20 dB, the PSLR reached 46.7 dB (top row). At an SNR level of 0 dB, the PSLR reached 25.7 dB (center). At low SNR level of -20 dB the PSLR is degraded to 8 dB (bottom row), though main lobe remains discernible.

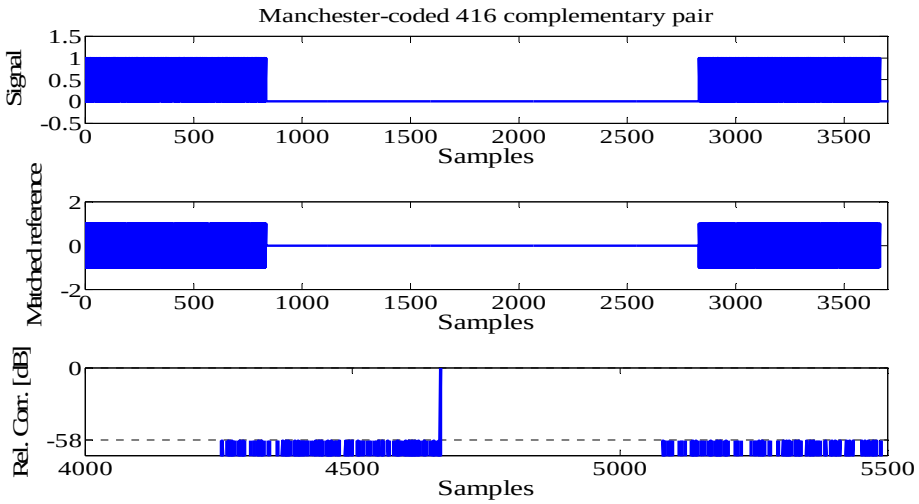

Figure 2.12 Transmitted code *T* (top) and match-filter code *R* (center) corresponding to the 416 bits-long complementary pair code. Bottom – aperiodic cross-correlation between the transmitted code *T* and the matched-filter code *R*.

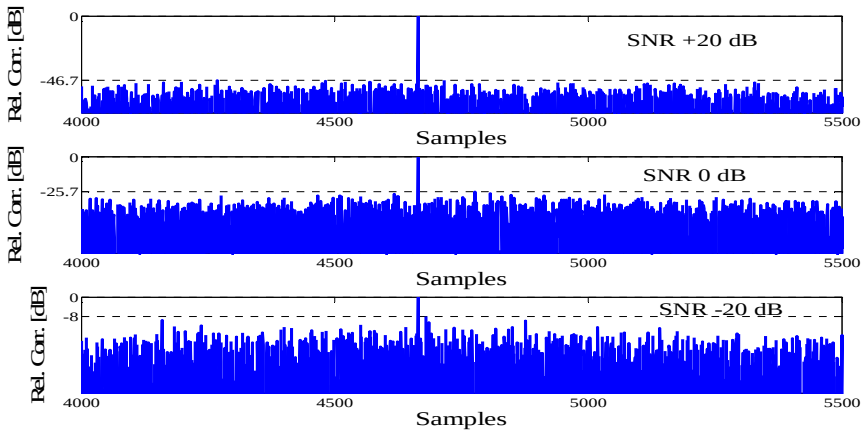

Figure 2.13 Cross-correlations of an incoherently compressed, 416 pulses-long complementary code. Top row: simulated compression with a signal-to-noise ratio of +20 dB. Center row: simulated compression with a signal-to-noise ratio of 0 dB. Bottom row: simulated compression with a signal-to-noise ratio of -20 dB.

2.5.4. 832 bits-long complementary pair

Lastly, 832 bits-long complementary pair codes were simulated. The code was generated by applying the complementary pair creation rule to the 26 element primitive pair of Table I five times (2^5 x 26 = 832; see Section 1.3, Chapter 1). The transmitted Manchester coded sequence *T* is illustrated in Fig. 2.14 (top), alongside its

matched reference R (center). Following the enlargement of the code length by factor of 2, the noise-free aperiodic cross-correlation between R and T has a PSLR of 64 dB (Fig 2.14 bottom).

Again, sidelobe suppression at +20 dB, 0 dB, and -20 dB SNR levels are illustrated in Fig. 2.15. At a high SNR of 20 dB, the PSLR reached 50 dB (top). At an SNR level of 0 dB, the PSLR reached 29 dB (center). At low SNR level of -20 dB the PSLR is degraded to 13 dB (bottom).

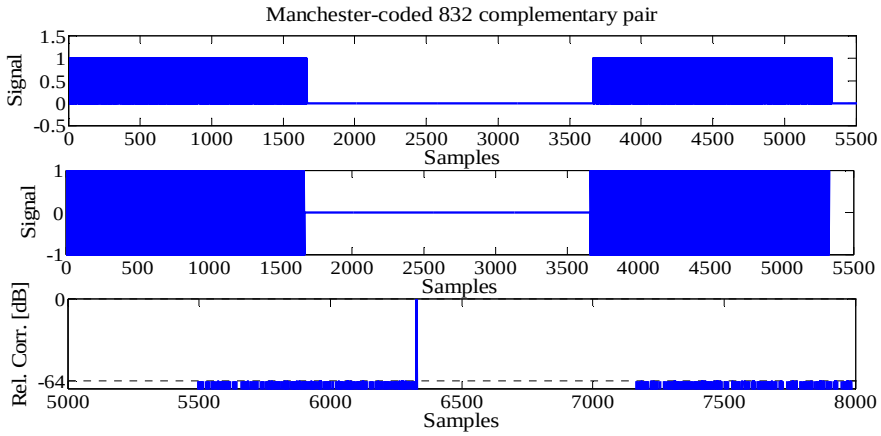

Figure 2.14 Transmitted code T (top) and matched filtering code R (center), corresponding to the 832 bits-long complementary pair code. Bottom – aperiodic cross-correlation between the transmitted code T and matched filtering code R.

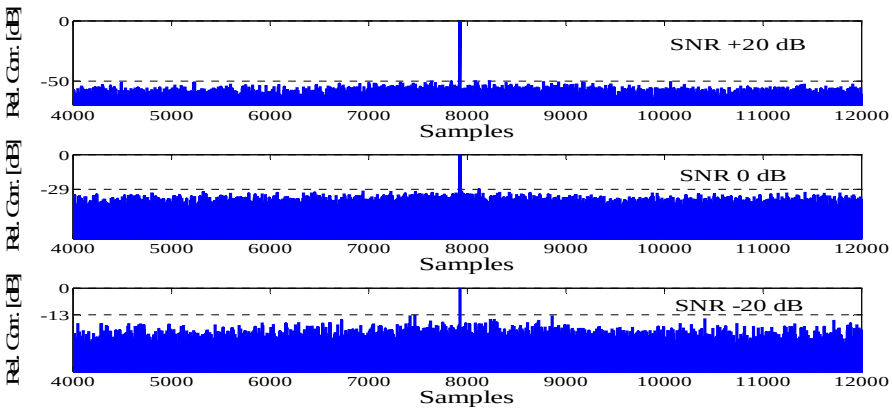

Figure 2.15 Cross-correlations of an incoherently compressed, 832 pulses-long complementary code. Top: simulated compression with a signal-to-noise ratio of +20 dB. Center: simulated compression with a signal-to-noise ratio of 0 dB. Bottom: simulated compression with a signal-to-noise ratio of -20 dB.

2.6. Experimental sidelobe suppression

The set-up for laser ranging measurements using incoherent pulse compression is shown in Fig. 2.16. Light from a laser diode at 1550 nm wavelength passed through a Mach-Zehnder electro-optic intensity modulator (MZM), driven by an arbitrary waveform generator programmed to the transmission sequence T. The average transmitted power was 100 mW and the collimating lens aperture was 25.4 mm. The sequence was constructed from a 1112 bits-long minimum peak-to-sidelobe ratio (MPSL) bipolar code or from 832 bits-long complementary pair code, following the above procedure. The coding symbol duration was 200 ps. The codes were repeatedly transmitted every 2 μs-long intervals. The measurement SNR was controlled by the addition of ASE of variable power from an EDFA.

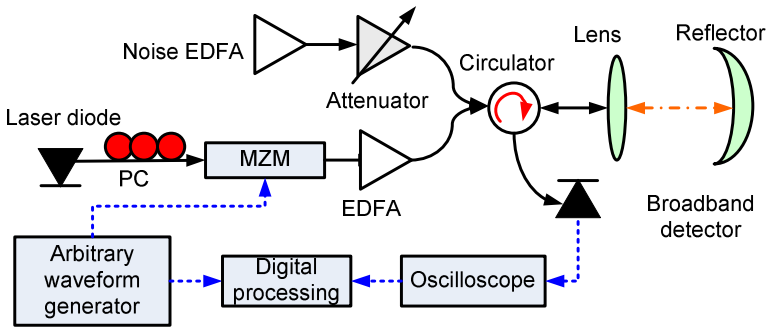

Figure 2.16 Experimental setup for LADAR measurements using incoherent pulse compression. MZM: Mach-Zehnder modulator. PC: polarization controller. EDFA: erbium-doped fiber amplifier. Black solid lines denote fiber connections, blue dashed lines represent electrical cables, and orange dash-dotted lines describe free-space propagation.

The modulated waveform was amplified by a second EDFA and launched towards a movable retro-reflector via a fiber circulator with 55 dB isolation and a collimating lens. Reflections were partially collected by the lens, directly detected by a photodiode with 12 GHz bandwidth, and sampled by a digitizing oscilloscope of 6

GHz bandwidth. The detected sequences were compressed through matched and mismatched filtering, carried out using offline signal processing.

In a first set of experiments, the retro-reflector was placed a short distance (tens of cm) from the lens, and the detection SNR was varied through adjusting the power of both the laser diode and ASE noise source. In this manner the reflected signal remained above the thermal noise of the photodetector, and the SNR was quantified by switching the ASE noise on and off.

First, 1112 bits-long MPSL code was used as the transmitting signal T. The cross-correlations of incoherently compressed LADAR are shown in Fig. 2.17, alongside the simulated correlations of compressed noise-free sequences. At a high SNR of +20 dB, the PSLR of the experimentally obtained sequence following matched filtering reached 33 dB, in agreement with the design prediction. A mismatched filter further improved the PSLR to 46 dB, while the peak power of the main correlation lobe was only 1 dB lower than that obtained with a matched filter. The results come close to the simulated 43 dB PSLR of the mismatched MPSL code (see Fig 2.11 top row).

Incoherent compression could still be carried out even when the measurement SNR was drastically degraded to -20 dB (Fig. 2.17, bottom row) in a good agreement with the simulation results (see Fig. 2.11 bottom row). Here the sidelobe suppressions obtained with matched and mismatched filters were practically equal, as the added value of the mismatched filter was overshadowed by the intense additive noise. The results demonstrate the potential of the incoherent compression scheme at poor SNR conditions.

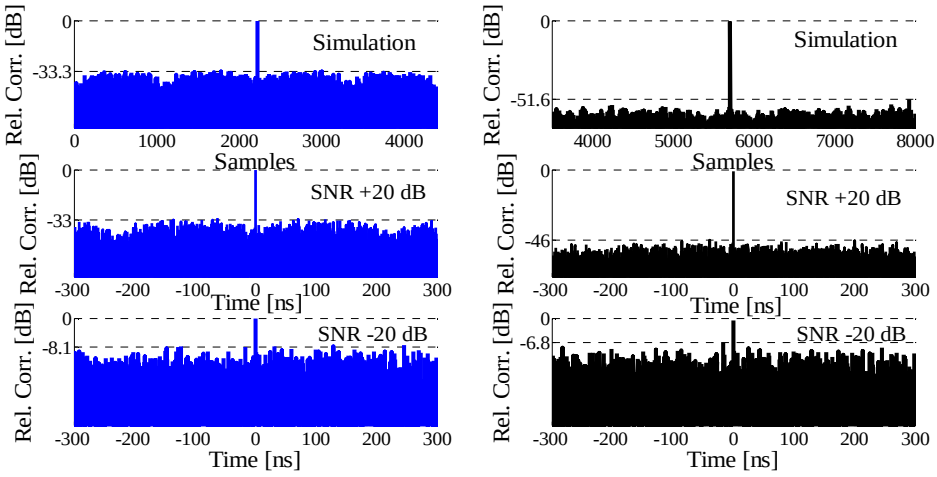

Figure 2.17 Cross-correlations of an incoherently compressed, 1112 pulses-long unipolar sequence. Both matched (left, blue) as well as mismatched (right, black) filters were used in the compression process. Top row: simulated compression of noise-free sequences. Center row: compression of experimentally obtained LADAR echoes, detected with a signal-to-noise ratio of +20 dB. Bottom row: compression of experimentally obtained LADAR echoes, detected with a signal-to-noise ratio of -20 dB.

Next, the matched-filtered, incoherent compression of complementary code pairs was demonstrated in a laser rangefinder experiment. The 832 bits-long complementary pair code was used as the transmitting signal T. The cross-correlations of incoherently compressed LADAR are shown in Fig. 2.18, alongside the simulated correlations of compressed noise-free sequences. At a high SNR of +20 dB, the PSLR of the experimentally obtained sequence following matched filtering reached 42 dB (see Fig 2.18, center). The sidelobe suppression is an order of magnitude better than that of a longer match-filtered MPSL sequence. The comparable incoherent compression of the MPSL sequence required a precise mismatched filter of 3336 coefficients [44]. Once again, compression could still be carried out at SNR level of -20 dB. The PSLR in this case degraded to 10 dB (Fig 2.18, bottom) in a good agreement with the simulation results (see Fig. 2.15 bottom).

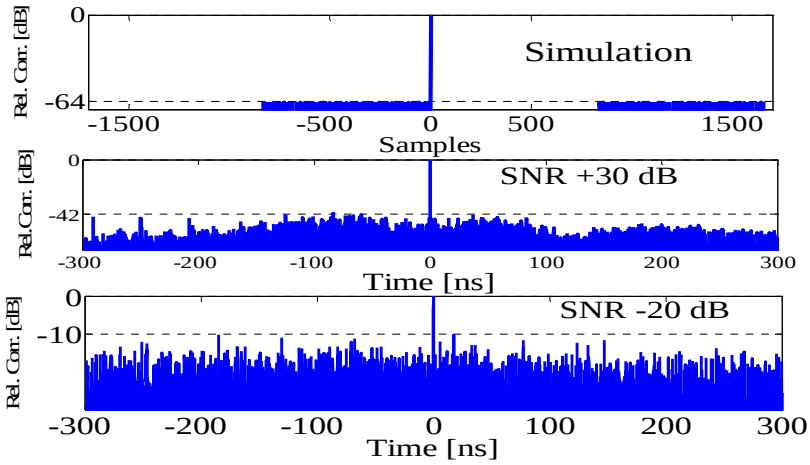

Figure 2.18 Cross-correlations of an incoherently compressed, 832 pulses-long complementary code. Top: simulated compression of noise-free sequences. Center: compression of experimentally obtained LADAR echoes detected with a signal-to-noise ratio of +20 dB. Bottom row: compression of experimentally obtained LADAR echoes detected with a signal-to-noise ratio of -20 dB.

The full width at half maximum of the main correlation lobe, signifying resolution, is 200 ps as expected. The results illustrate the simple scaling of the proposed principle and carry a promise for high performance in simple-architecture laser range-finders and other photonic systems.

2.7. Laser range-finder measurements

Preliminary ranging performance was illustrated by placing the retro-reflector several distances away from the collimating lens. The 1112 bits long MPSL code was used. The average transmitted power was 100 mW, the collimating lens aperture was 25.4 mm, the symbol duration was 200 ps and the sampling interval of the digitizing oscilloscope at the output of the receiver was 50 ps. First, the retro-reflector was placed 6 meters away from the collimating lens.

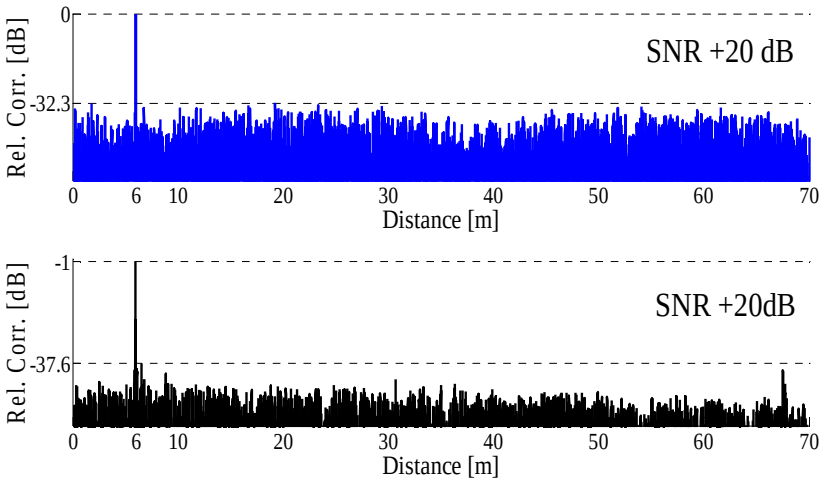

Figure 2.19 Experimental cross-correlations of an incoherently compressed, 1112 pulses-long unipolar sequence collected from a reflector that was placed 6 m away from the collimating lens at an optical SNR of +20 dB. Top: compression using matched filter. Bottom: compression using mismatched filter**.**

The SNR of the collected reflection was 20 dB. Both matched and mismatched filters were used in the pulse compression. Fig 2.19 displays the compressed waveforms as function of absolute distance. The PSLR for the matched and mismatched filters were 32.3 dB and 36.6 dB respectively with mismatch-induced loss of 1 dB.

Next, the retro-reflector was placed 50 meters away from the collimating lens, and the SNR of the collected reflection was +18 dB. Fig 2.20 displays the compressed waveforms as function of absolute distance. The PSLRs this time were 31.7 dB and 38.2 dB respectively, with 1 dB induced mismatch loss.

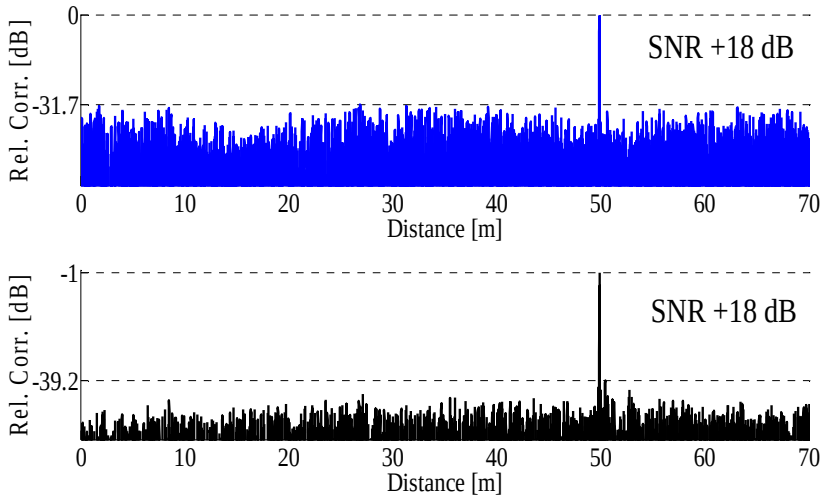

Figure 2.20 Experimental cross-correlations of an incoherently compressed, 1112 pulses-long unipolar sequence collected from a reflector that was placed 50 m away from the collimating lens at an optical signal to noise ratio of 18 dB. Top: compression using matched filter. Bottom: compression using mismatched filter.

Lastly the ranging precision of the system, defined by its ability to recover relative changes in the distance of a single target, was evaluated by placing the reflector 50 m away from the collimating lens, and changing its position by 2.5 cm. Fig. 2.21 displays the compressed waveforms as function of delay for the two reflector positions. A mismatched filter was used in the compression process. The full width of the mainlobe at 70 dB below the peak is approximately 4 cm, in agreement with the pulse duration and sampling rate. The PSLR of both curves is above 35 dB. The two peaks are approximately 2.4 cm apart, in agreement with the reflector position change.

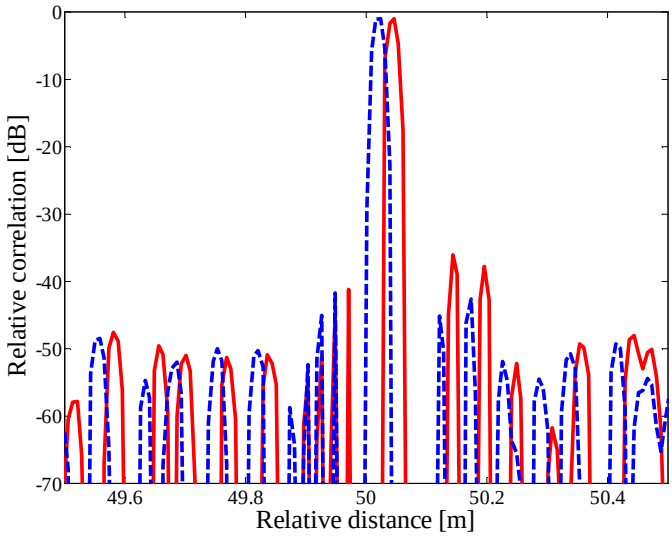

Figure 2.21 Cross-correlations of incoherently compressed, 1112 pulses-long unipolar LADAR echoes. The distances between the LADAR lens and a retro-reflector were 50 m (blue, dashed) and 50.025 m (red, solid). The measurement SNR was 18 dB. A mismatched filter was used in the compression.

2.8. Concluding remarks

In this chapter, a LADAR system based on incoherent pulse compression was proposed and demonstrated. The system relies on simple intensity modulation and direct detection of dense position-coded MPSL sequences and complementary code pairs. The compression is achieved through cross-correlating the received echoes with matched or mismatched filters stored at the receiver. The principle is of particular consequence for photonic applications, in which coherent detection is more difficult to implement. A PSLR of 46 dB was achieved for mismatched filtered, 1112 bits long MPSL code, and 42 dB for matched filtered 832 bits long complementary pair. The spatial resolution of the experimental demonstration is estimated as 3 cm. A change in range of 2.5 cm was accurately recovered in a high-SNR measurement. The ranging accuracy for SNR of 20dB and transmitted pulse width of 200ps is estimated as 2 mm. The systems link budget suggests a maximum operating distance of about 100 m

(without averaging), limited primarily by the detector noise and the maximum transmitted power. Averaging can further extend the maximum operating distance.

Until this stage, the compression principle was demonstrated based on reflections from a retro reflector that was placed in front of the ranging transmitter. In the next chapter, ranging measurements to a realistic Lambertian reflecting target are reported, which further substantiate the applicability of the proposed technique.

CHAPTER

3

Incoherent pulse compression from a realistic target

3.1 Incoherent pulse compression from a realistic Lambertian reflecting target

This chapter presents laser ranging measurements to a realistic Lambertian reflecting target, using incoherent pulse compression of various sequences. The bipolar codes are converted to unipolar representations using the pulse position modulation algorithm, and used in intensity modulation of a laser ranging source, as was described in subsection 2.4.1. The reflected echoes from a target are directly and incoherently detected and the range to the target is extracted based on cross-correlation with a reference sequence. Calculations of the compressed forms a of 416 bits-long code pair and 1112 bits-long MPSL code in the presence of additive noise and at different ESNR levels are provided in section 2.5. While the initial experiments demonstrated the compression principle (see section 2.6), they nevertheless relied on a reflection form a retro reflector placed in front of the ranging transmitter.

Two classes of phase codes were employed in laser ranging experiments of realistic targets. In a first set of "short range" experiments, we have demonstrated the incoherent pulse compression of a pair of 416 bits-long complementary codes (section

3.2). Ranging measurements towards the white walls of the laboratory were successfully preformed in the presence of additive noise at ESNR values of -20 dB [49]. In a second "long range" set of measurements, we used 416 bits-long complementary code pairs as well as 1112 bits-long MPSL that were transmitted to a maximum distance of 70m. The experiments were carried out in the corridor of the Faculty of Engineering building. The target was a white paper poster mounted on movable chassis. The PSLR in the experiments was in agreement with predictions. Here too, incoherent compression was successfully carried out at ESNR values as low as -20 dB. The distance to the target could be recovered based on weak collected echoes, with an average optical power as low as 3 nW, without averaging over repeating measurements.

3.2 Short range realistic target experimental setup and results

The experimental setup for laser ranging measurements using the incoherent compression of a complementary code pair is shown in Figure 3.1. Light from a laser diode at 1550 nm wavelength passed through a Mach-Zehnder electro-optic intensity modulator (MZM), driven by an arbitrary waveform generator programmed to the transmission of the code pair. The coding symbol duration was 1 ns, corresponding to an expected spatial depth resolution on the order of 15 cm. The 416 bits-long codes used in the experiment were the same as those of the simulations (Chapter 2, section 2.5.3). The codes were repeatedly transmitted every 6 μs, with the interval between the complimentary pairs equal to 3us. The modulated waveform was amplified by an erbium-doped fiber amplifier (EDFA) to an average output power of +23 dBm, and

launched towards a white wall through a collimating 2" lens. The distance to the wall was 8 m.

The relative reflectivity ρ_t of the white wall target was evaluated in the following manner: a laser beam of known power was launched towards the target wall from few cm range at a known angular offset $+\theta$ from normal incidence, and a free-space integrating sphere power meter was placed as close as possible to the wall at the opposite angle $-\theta$ of specular reflection. The power meter was able to collect the vast majority of scattered power, whose angular scatter is centered at the direction of specular reflectance $-\theta$. The measurements provided an estimate of ρ_t equal to 7%.

Reflections from the wall were partially collected by a telescope mirror of 20 cm aperture into a multimode fiber with a core diameter of 200 μm, and detected by an InGaAs APD. The bandwidth of the APD was 1 GHz, and its NEP at that bandwidth was -43 dBm. The output of the APD was sampled by a real-time digitizing oscilloscope of 6 GHz analog bandwidth, and the detected sequences were incoherently compressed through digital match-filtering of both codes, using the corresponding bipolar reference sequences as described in the previous chapter. The cross-correlation of the two codes were then added together to obtain a ranging measurement with low sidelobes.

The average optical power of the collected reflection echoes was -41 dBm, representing an estimated ESNR of +4 dB. The collected power is approximately 14 dB lower than expected, due to alignment difficulties and transmission losses at the coating of the telescope mirror. Further, the transmitted optical power was lowered through reducing the output power of the EDFA in order to measure the PSLR at different SNR scenarios.

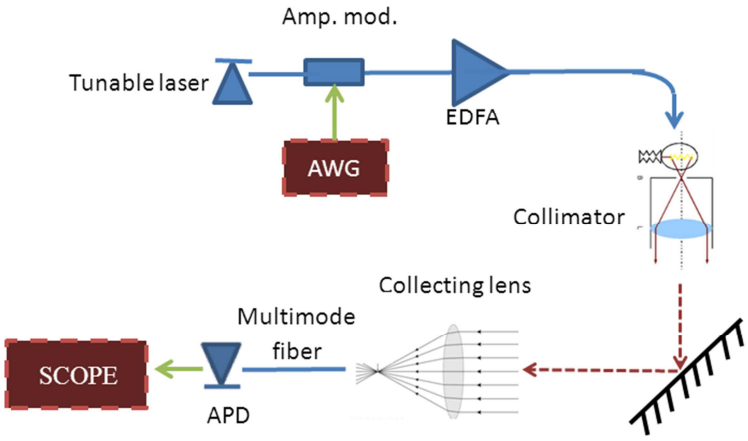

Figure 3.1 Experimental setup for laser ranging measurements using incoherent pulse compression of complementary code pairs. APD: avalanche photo diode. $Amp.mod.$: amplitude modulator. AWG: arbitrary waveform generator. $EDFA$: erbium-doped fiber amplifier. Blue solid lines denote optical fibers; green solid lines denote radio-frequency electrical cables; dashed, red lines denote free-space propagation.

Figure 3.2 shows the experimentally obtained, incoherently compressed code pair echoes. The traces shown in the four panels correspond to average received optical power levels of -41 dBm, -47 dBm, -50 dBm and -53 dBm. The distance to the reflecting wall target is clearly identified in all traces, with PSLR values of 28 dB, 18 dB, 13 dB and 8 dB, respectively. Ranging measurements at ESNRs below -20 dB required averaging over multiple repetitive transmissions of the two codes. Figure 3.3 shows the incoherently compressed code pair detected at an average optical power of -63 dBm, following 1024 averages. The range to the target was measured with a PSLR of 20 dB.

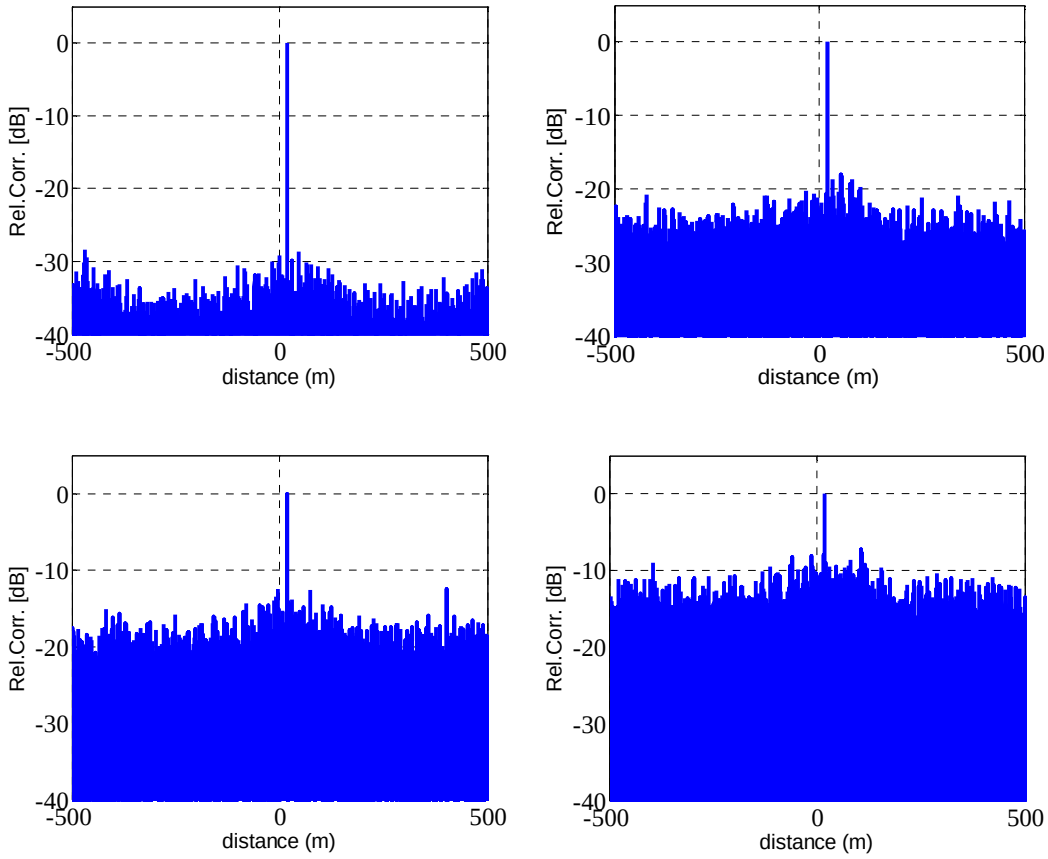

Figure 3.2 Incoherently compressed forms of experimentally obtained complementary code pairs, reflected from a white wall located 8 m away from the laser range-finder. The length of each code in the pair was 416 bits. The duration of each transmitted symbol was 1 ns. The average optical power levels of the collected echoes were -41 dBm (top left), -47 dBm (top right), -50 dBm (bottom left), and -53 dBm (bottom right). The distance to the target could be resolved in all measurements. The corresponding PSLR values were 28 dB, 18 dB, 13 dB and 8 dB, respectively.

The results are in a good agreement with the simulations performed in Chapter 2, subsection 2.5.3. The obtained PSLRs of 28 dB at -41 dBm optical power level (ESNR = 4 dB), and of 8 dB at -53 dBm optical power level (ESNR = -20 dB), agree well with the corresponding simulation predictions.

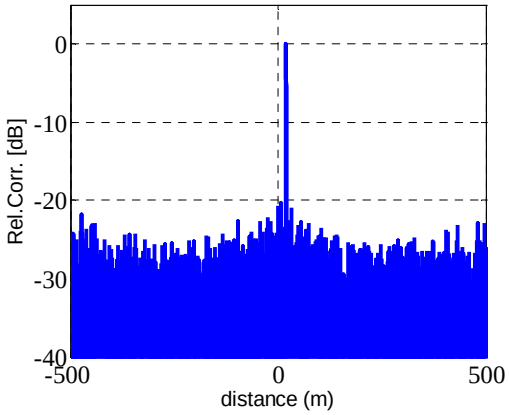

Figure 3.3 Incoherently compressed form of an experimentally obtained complementary code pair, reflected from a white wall located 8 m away from the laser range-finder. The length of each code in the pair was 416 bits. The duration of each transmitted symbol was 1 ns. The average optical power level of the collected echoes was -63 dBm, and the received waveform was averaged over 1024 repetitions. The distance to the target could be resolved with a PSLR value of 20 dB.

3.3 Comparison of experimental and predicted link budgets

As discussed in section 2.3, the solid angle θ_R over which radiation is dispersed from a Lambertian target takes the value of π steradians. Following the expression obtained in section 2.3 (equation 2.10, reprinted here for convenience with addition of a coupling loss factor), the expected optical power collected at the receiver can be estimated as:

$$P_r = \frac{P_t \cdot \tau_L \cdot D_R^2 \cdot \rho_t}{4 \cdot R^2} \tag{3.1}$$

Where P_t is the transmitted optical power (23 dBm), D_r is the receiver circular aperture (20 cm), ρ_t is the target reflectance parameter (0.07) and R is the one-way distance to the object (8 m). Substituting the above parameters into equation, we find that the excess coupling loss of the setup (τ_L) is about 14 dB. The setup should be modified to reduce these excess losses (see a next section).

The experimental results suggest that a lowest ESNR in which the correlation peak could still be observed without averages over repeating patterns is -20 dB, corresponding to a received optical power P_r of -53 dBm at the input of the APD. When 1,024 averages were used, a good PSLR of 20 dB was obtained for a received optical power P_r of only -63 dBm (corresponding to an ESNR of -40 dB without averaging). Averaging improves the ESNR by $20 \cdot \log(1024)$ = 30 dB, to the order of -10 dB. The observed PSLR is an agreement with expectation for this ESNR level. The ESNR and PSLR levels for P_r of -53 dBm and -63 dBm are summarized in Table 3:

TABLE 3 Signal-to-noise improvement by averaging process

Pin [dBm]	ESNR [dB]	PSLR [dB]
-53, no averaging	-20	~8
-63, no averaging	-40	N/A
-63 with 1,024 averages	-40 + 30 = -10	~20

3.4 Ranging measurements to a realistic target at 70 m distance

Prior to a second set of experiments, the optical paths of both transmission and receiving were improved to reduce the excess coupling losses of the setup. The collimating lenses on both paths were replaced by high-quality aspheric lenses of 10 cm diameters. The lenses were mounted on mechanical benches which allowed for precise, three-axis position adjustments. The transmitted optical power this time was 21 dBm and the distance to the target was varied between 20-70 m. Figure 3.4 shows the experimentally collected optical power levels at different distances, alongside the corresponding predicted values. The results show that coupling losses were effectively reduced to a marginal value of 1 dB.

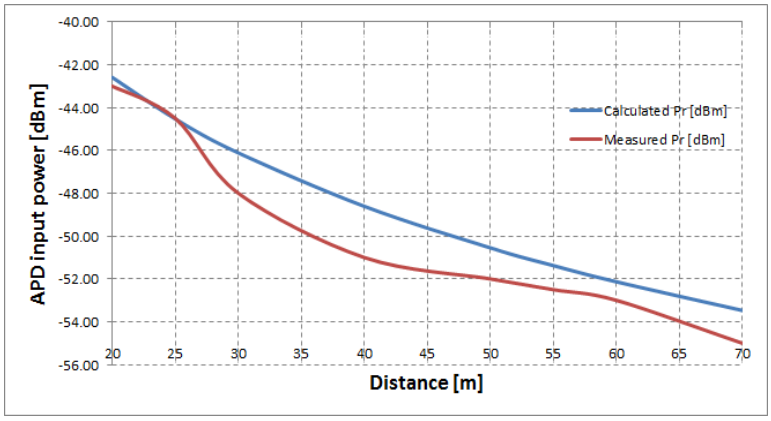

Figure 3.4 Measured and calculated received optical powers as a function of distances.

Next, ranging measurements were performed using the 416 pulses-long complementary code pair and the 1112 pulses-long MPSL sequence. The duration of each transmitted symbol was 1 ns and the distance to a white poster target was 70m, limited by the length of the corridor. The transmitted optical power at the collimating lens output was varied between 19-21 dBm. The corresponding, received optical power levels were between -55 and -53 dBm. Subject to the experimental conditions, a transmission power of +21 dBm resulted in a ESNR of -20 dB, the minimal value required for reliable ranging measurements. Figure 3.5 (top row) shows the incoherently compressed forms of the collected echoes, for the complementary code pair and the MPSL. Valid measurements were obtained in both cases, with PSLR values of 8 dB and 9 dB.

The bottom row of Fig. 3.5 shows the incoherently compressed form of reflected echoes, collected when the transmitted power was reduced to +19 dBm (ESNR of -24 dB). The PSLR was 2.5 dB and 3.5 dB for the two codes. These PSLR values are too low to be considered acceptable.

Figure 3.6 shows the incoherently compressed form of the 416 pulses-long complementary code pair, collected at an ESNR of -26 dB and following 256 averages

over identical patterns. The averaging improves the ESNR of an effective value of -2 dB. The range to the target was measured with a PSLR of 25 dB, in agreement with calculations. Again, the measured result fit the theoretical value and shows that the working distance can be further increased: the SNR improvement of 24 dB boost the PSLR to an easily discernible value.

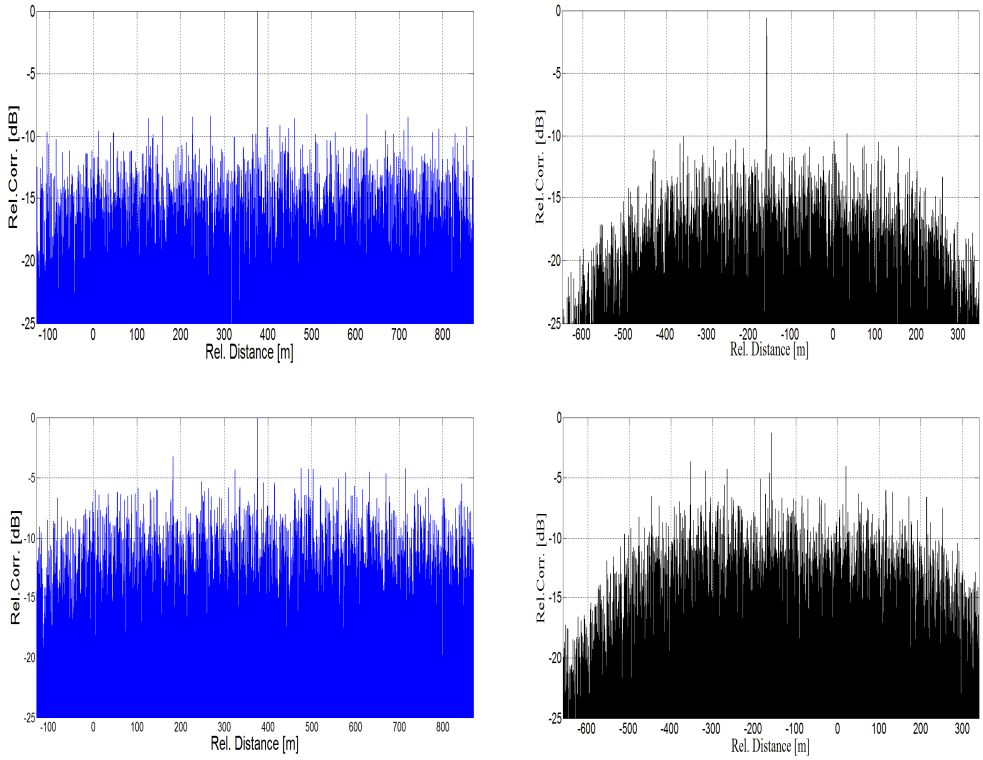

Figure 3.5 Experimental cross-correlations of incoherently compressed, MPSL (black color) and complementary code pairs (blue color) unipolar sequences, reflected from a white poster located 70 m away from the laser range-finder. The length of complementary code in each pair was 416 bits and the used MPSL consisted of 1112 pulses. The duration of each transmitted symbol was 1 ns and the transmitted optical powers were 21dBm (top row) and 19dBm (bottom row). The average optical power levels of the collected echoes were -53 dBm (top left and right), and -55 dBm (bottom left and right). The corresponding PSLR values were 8 dB, 9 dB, 3.5 dB and 2.5 dB, respectively. The distance to the target could be resolved reliably only in the measurements of the top row. The mismatch filter losses are 0.59dB (top right) and 1.27dB (bottom right).

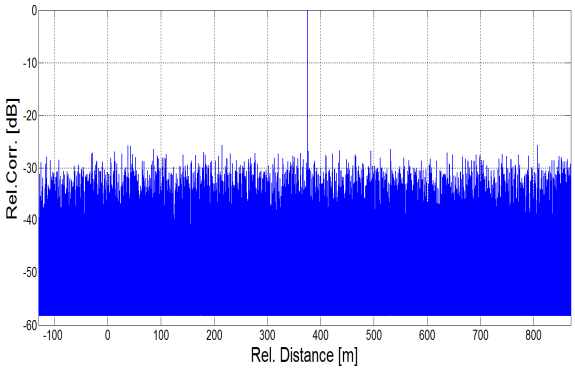

Figure 3.6 Incoherently compressed form of an experimentally obtained complementary code pair, reflected from a white poster located 70 m away from the laser range-finder. The length of each code in the pair was 416 bits. The duration of each transmitted symbol was 1 ns. The average optical power level of the collected echoes was -56 dBm, and the received waveform was averaged over 256 repetitions. The distance to the target could be resolved with a PSLR value of 25 dB.

3.5 Chapter conclusion

Ranging measurements using incoherent pulse compression were demonstrated experimentally. The results were extended to the processing of echoes reflected from a realistic target. The large gain provided by the implemented codes allows for the processing of very weak reflected echoes. The range to the target could be recovered even when the optical power of the received signal was -53 dBm, or 10 dB below the NEP of the APD used, without averaging over repeating patterns. The processing gain of incoherent pulse compression can be leveraged towards laser ranging systems with smaller receiver apertures and/or reduced transmitted power and energy consumption. Low-power ranging systems which take advantage of a strong processing gain would be better immune against interception and jamming by an adversary.

The experiments reported above demonstrated successful ranging up to a distance of 70 m. The transmitted optical power that was necessary to perform the measurement without averages was +21 dBm (125 mW) and the duration of the measurement was only 2.5 microseconds.

This transmitted power is only 1 dB lower than the maximum power that could be launched using the presently available EDFA. Therefore the maximum range that can be currently measured without averages is about 80-90 m. There are several feasible solution paths, however, for extending the measurement range:

- Direct splicing of the EDFA output fiber to the transmission collimator. Potential improvement with respect to current experiment: 5 dB (the maximum output optical power of EDFA in use is +26 dBm).
- Using of EDFA with higher output power. Potential improvement with respect to current experiment: 14 dB (state-of-the-art high power EDFAs can allow more than +40 dBm of output optical power).
- Increase of the collection aperture from 10 cm (4") to 25 cm (10"). Potential improvement with respect to current experiment: 8 dB.

With implementing all three solutions, the optical power collected by the receiver may be increased by a factor of about 500 (27 dB). Given such improvement, the marginal ESNR of -20 dB can be reached for a target range that is about 20-21 times longer than the 70 m of the current experiment, towards 1.4 km. Further increase in range towards few kilometers would have to rely on the extension of the transmission duration in one of the two following ways, or via a combination of both: Increasing the length of the codes, and/or averaging over a number of repetitions. A three-fold increase in range from 1 km to 3 km, for example, reduces the collected optical power by a factor of 10 and the ESNR by a factor of 100. The ESNR can be recovered by increasing the length of the code by a factor of 100, towards 100,000 bits, or by employing about 100 averages. An illustrative example of the benefit of averages is seen in Figures 3.6, where 256 averages were used. The 70 m range to the

target could be measured with PSLR that was better than 25 dB, whereas the range could not be recovered at all with the same transmitted power but without averages.

The transmission duration of codes that are 100,000 bits long would be several hundreds of micro-seconds. While complementary code pairs can be scaled to such lengths, the experimental realization of measurements based on such long codes might run into difficulties in pattern generation, sampling, and the transfer and processing of data using current equipment. It is therefore likely that a combination of longer codes alongside averaging over tens of repetitions should be employed instead in the next sets of experiments. Averaging induces dead-time overheads between repeating transmissions, which are likely to extend the overall transmission duration to the order of milliseconds.

The next chapter (Chapter 4) addresses potential upgrades of an incoherent LADAR system, and the possibility of acquiring 3D images. So far, the provided simulations and experiments have been limited to a “0-D” ranging system (that is, the depth measurement of single point). Acquisitions of 3D images would require a fast and precise angular scanning capability in two dimensions in order to create a range image. The corresponding metrics will be discussed.

Experiments thus far were carried out inside university walls, at indoor conditions. When going outdoors, atmospheric effects that change the air refractive index should be considered as well. The air refractive index is primarily a function of atmospheric pressure, temperature, and humidity. These sources of uncertainty, and methods for avoiding and correcting these errors, are also addressed in Chapter 4.

CHAPTER

4

Research Discussion and Summary

4.1. Summary

In this research, high-resolution laser ranging system with strong sidelobe suppression was proposed and demonstrated experimentally. The sidelobe suppression was obtained through an incoherent pulse compression process that was proposed by Prof. Nadav Levanon of Tel-Aviv University. The compression relies on the transmission and direct detection of Manchester coded, unipolar representations of a chosen binary phase sequence, and its matched or mismatched filtering by a stored bipolar reference on receive. The extent of sidelobe suppression nearly replicates that of the original bipolar sequence, even though phase is not maintained and a simple incoherent receiver is employed. This principle is of particular interest for photonic applications, in which coherent detection is more difficult to implement.

Simulation and experiments demonstrated ranging measurements to a white wall target located up to 70 m away, at a negative ESNR of -20 dB, using a modest transmitted power of only 200 mW, with the acquisition time of only few micro-seconds and without averages. Two different coding sequences were employed, with similar performance: one was drawn from a 1112 bit-long bipolar MPSL sequence, and the other constructed from a complementary pair of 416 bit-long sequences. The

noise tolerance of the proposed configuration can be leveraged towards a longer measurement range, lower launch power and energy consumption, reduced apertures and improved operation at unfavorable atmospheric conditions.

Range and resolution limitations were as follows: The system resolution was proportional to the duration of a single pulse in transmitted code sequence, and was set to 15 cm for the 70 m range measurements. The resolution was chosen to match that of typical airborne LADAR systems. The 1 GHz bandwidth of the APD was chosen to match that requirement. The theoretical sidelobe suppression at high SNR values scales with the length of the sequences used. In that respect complementary code pairs, whose lengths are arbitrarily scalable, are advantageous over MPSL sequences. In practice, however, PSLR is often limited by additive noise, primarily thermal and multiplication factor noise of the APD. The experimentally obtained ranging performance agrees with simulations. Range can be increased beyond 1 km with higher transmission power, larger receiver aperture, longer code pairs, compromising resolution, and/or averaging over numerous repetitions. Tradeoffs among these parameters are addressed in the next section.

4.2. Parameter tradeoffs

In this subsection, I illustrate the tradeoff among range, resolution, transmitted power, aperture size and length of code in an incoherently-compressed laser range finder.

On the one hand, the signal-to-noise considerations can be expressed as follows: $OSNR = \frac{P_r}{NEP \cdot \sqrt{B}}$, $ESNR = \frac{P_r^2}{NEP^2 \cdot B}$, where $OSNR$ and $ESNR$ denote the optical and electrical signal-to-noise ratios respectively, B is the detection bandwidth,

and NEP is the noise-equivalent power of the detector in units of Watt per Hz$^{1/2}$. NEP is defined so that an $ESNR$ of unity is obtained when the received optical power P_r equals $NEP \cdot \sqrt{B}$.

On the other hand: the resolution is given by $\Delta z = \frac{c}{2B}$. Hence:

$$ESNR = \frac{P_r^2 \cdot 2\Delta z}{NEP^2 \cdot c} \tag{4.1}$$

Further, the collected optical power equals $P_r = \frac{D_r^2 \cdot \rho}{4R^2} \cdot P_t$, where ρ is the relative power reflectivity of the target surface, D_r is the diameter of the receiver lens aperture, R is the range to the target, and P_t is the transmitted optical power at the output of the ranging system. Putting it all together:

$$ESNR = \frac{D_r^4 \cdot \rho^2}{16R^4 \cdot NEP^2 \cdot c} \cdot 2\Delta z \cdot P_t^2 \tag{4.2}$$

The maximum range R_{max} is obtained when the ESNR is reduced to its minimum tolerable value, $ESNR_{min}$:

$$ESNR_{min} = \frac{D_r^4 \cdot \rho^2}{16R_{max}^4 \cdot NEP^2 \cdot c} \cdot 2\Delta z \cdot P_t^2 \tag{4.3}$$

Our experiment suggest that the value of $ESNR_{min}$, using a pair of complementary codes of 416 bit each, is approximately -20 dB (0.01). The selection is somewhat arbitrary, yet it provides useful performance estimates. The ESNR scales with the number of bits N_{bits}, so that: $ESNR_{min} = 0.01 \cdot \frac{832}{N_{bits}}$. Solving for the maximum range, one finds:

$$R_{max}^4 = \frac{D_r^4 \cdot \rho^2}{16 \cdot NEP^2 \cdot c \cdot ESNR_{min}} \cdot 2\Delta z \cdot P_t^2 = \frac{D_r^4 \cdot \rho^2}{16 \cdot NEP^2 \cdot c \cdot 8.32} \cdot 2\Delta z \cdot N_{bits} \cdot P_t^2$$

$$= \frac{D_r^4 \cdot \rho^2}{66.5 \cdot NEP^2 \cdot c} \cdot \Delta z \cdot N_{bits} \cdot P_t^2 \qquad (4.4)$$

Many of the parameters above represent constraints of our setup: NEP = 1.5 pW/Hz$^{1/2}$, D_r = 10 cm, ρ = 0.07, Δz = 15 cm. Plugging in these constants, the above trade-offs expression reduces to:

$$R_{max}^4 = 1.5 \cdot 10^6 \cdot N_{bits} \cdot P_t^2 \qquad (4.5)$$

For example, Figure 4.1 illustrates the maximum range as a function of transmitted power, using a complementary code pair, each 416 bits long. The range for the maximum 'reasonable' transmission power of 1 W is about 200 m.

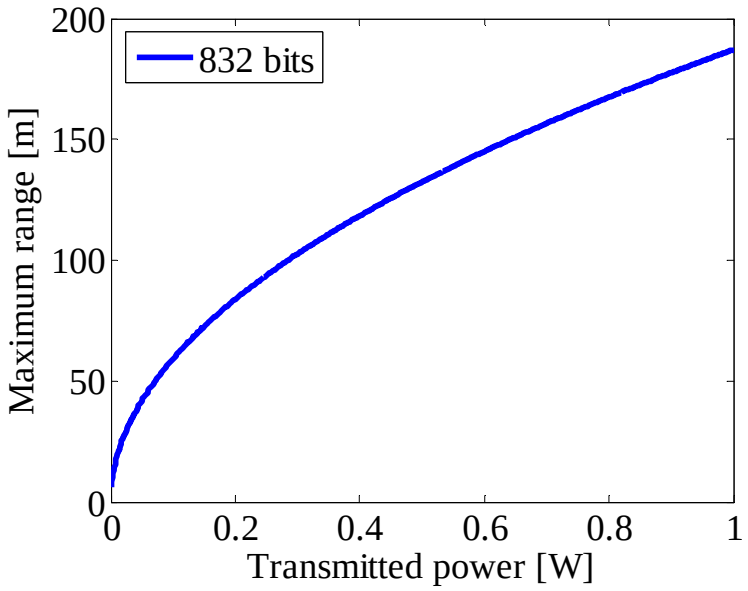

Figure 4.1 Maximum ranges as a function of transmitted power using a complementary pair of 416 pulses-long codes.

In the Figure 4.2, the maximum range is drawn as a function of number of bits in the code, assuming a transmitted power of 1 W. If we take a 1 km range requirement as a constraint, and 1 W transmission power as an upper limit, the code needs to be about 700,000 bits long. The measurement time would be about 1.4 ms.

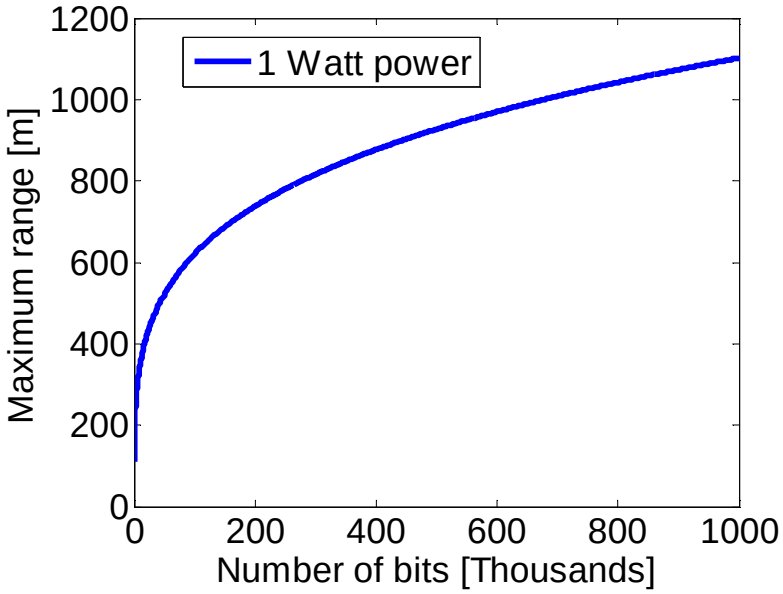

Figure 4.2 Maximum ranges as a function of number of bits in a complementary code pair. Transmission power of 1W is assumed.

If the code is not long enough, then averages are required. The number of bits in all averaged measurements combined would need to be 700,000. If the code has 700 bits, for instance, 1,000 averages would be required.

4.3. Comparison between time-of-flight and sequence compression

As discussed earlier in this dissertation, the resolution of ToF and sequence compression systems is in principle the same, provided that the duration of individual sub-pulses within the sequence matches that of the single pulse of the ToF configuration. When the overall transmitted energies of the two configurations are equal, their ranging performance in the presence of additive noise should be the same as well. The ranging sidelobes of a ToF systems, at noise-free operation, are ideally zero, whereas those of sequence compression configurations are non-zero but extremely weak. This theoretical difference cancels out, however, in the presence of even modest additive noise.

One major advantage of the sequence compression protocol is in the reduction of the peak power level that is transmitted, by a factor that equals the number of bits in the sequence. Lower transmitted power provides better safety, and also better immunity against interception and jamming by an adversary.

Another significant difference between the two approaches has to do with their engineering realizations. Driven by continuing progress of fiber-optic light sources, amplifiers and modulators, sequence compression-based LADAR systems at 1550 nm wavelength can be much smaller, lighter and lower-cost compared with their ToF counterparts. The experimental setup used in this work included external electro-optic modulators, driven by 1Gbit/s sequences. Direct modulation of the driving current of laser diode sources is also possible at this rate, reducing the size and complexity of the transmitter even further. In contrast, lights sources of ToF LADARs are typically pulsed fiber lasers, which are much more complex, bulky and expensive. Although certain specialty laser diodes are capable of generating intense and narrow isolated pulses with sufficient energy, their pulse repetition rates are restricted to tens of kHz. These rates are increasingly insufficient, in particular in emerging applications such as 2D scanning systems that are addressed later in this chapter.

The optical communication market proposes a large selection of low-cost, readily available components at 10 Gbit/s rates and higher. These could allow for sub-cm depth resolution, while maintaining a low peak power transmission. Higher modulation rates also make the use of longer codes more practical, and therefore enable ranging measurements at even lower ESNRs without averaging.

4.4. Atmospheric considerations

Through the course of this research we did not address the ranging system performance limitations that are due to atmospheric conditions. First, imperfect optics and scatter and turbulence in the atmosphere lead to an expansion of the illumination beam with range. Good industrial LADARs with near-diffraction limited optics achieve beam diversion angles of around 0.2 mrad. Even so, a finite beam diameter of around 20 mm is obtained at 100 m range [55]. Diffraction therefore sets a limit to lateral resolution in scanning LADARs.

The refractive index of air is primarily a function of atmospheric pressure, temperature, and humidity. For visible or near-infrared light, variations in the refractive index over modest distances are primarily a function of temperature gradients, with only small additional contributions from humidity and pressure variations. In the visible spectrum, a 1 ºC increase in air temperature lowers the refractive index by a little less than 1 ppm. Index variations associated with atmospheric turbulence lead to short-term fluctuations in the collected optical power, known as scintillations. Scintillations power drops are stochastic in nature, and could reach as much as 30 dB.

Methods for mitigating the effects of index fluctuations are discussed, for instance, in the NISTIR 7117 report by Stones et al [55]. The general problem of beam propagation through a turbulent medium, where the temperature distribution is given by a statistical distribution, can be treated using the Helmholtz scalar wave equation with the refractive index described statistically in terms of its power spectrum [58]. Additional atmospheric considerations such as spatial variations in the structure function and double-pass effects (enhanced backscatter) are discussed by

Andrews and Phillips [58]. Atmospheric effects have been incorporated into comprehensive LADAR models by Burton *et al.* [59]

4.5. Future work directions

Further work could extend incoherent LADAR systems capability towards 3D imaging. Acquisition of 3D images would require a fast and precise angular scanning capability in two dimensions. A 3D scanner is a device that analyzes a real-world object or environment to collect data on its shape. The collected data can then be used to construct digital three-dimensional models. The purpose of a 3D scanner is to create a cluster of geometric samples on the surface of the object. These points can then be used to extrapolate the shape of the object (a process called *reconstruction*). A 3D scanner collects distance information about surfaces within its field of view. The "picture" produced by a 3D scanner describes the distance to a surface at each point in the picture. This allows the three dimensional position of each point in the picture to be identified.

An *active 3D laser scanner* uses laser light to probe the subject. At the heart of this type of scanner is a laser rangefinder. The laser rangefinder finds the distance of a surface by methods described in Chapter 1. The laser rangefinder only detects the distance of one point in its direction of view. Thus, the entire field of view is scanned one point at a time by changing the rangefinder's direction of view. The viewing direction of the laser rangefinder can be changed either by rotating the range finder itself, or by using a system of rotating mirrors. The latter method is commonly used because mirrors are much lighter and can thus be rotated much faster and with greater

accuracy. Typical 3D laser scanners can measure the distance of more than 100,000 points every second.

Many different technologies can be used to build 3D-scanning devices. Each technology comes with its own limitations, advantages and costs. Most LADAR systems must sequentially illuminate each pixel in a range image. A number of scanning technologies are available today: *single beam* scanners, *polygonal* scanners, *galvanometric* scanners, *acousto-optics* scanners, *electro-optic* scanners, *holographic* scanners, *tilt platform* scanners, and *beam array* scanners [60-66]. The latter one is probably the most interesting due to its small dimensions, ultra-light weight and rapidly steering capabilities.

The mirrors, prisms, and spinning polygons used decade ago are all made of precision glass or ceramics in forms controlled by macro fabrication technology. Their large mass and size impose limits to achievable angular deflection rates. Microfabrication process available today point the way onward. With reduced size comes reduced inertia, which in turn permits faster scanning and opens avenues to mass fabrication.

In the consumer market, the requirements for fast scanning could be very severe. For example, in order to provide video graphics array (VGA) with 480 x 640 pixel resolution and at 30 frames per second, the scanner must make 9.2 million ranging measurements per second. The duration of an individual measurement is therefore only ~100 ns. The high repetition rate prohibits the application of most pulsed laser sources. Elaborate modulation schemes of CW sources in needed instead.

For more than a decade the research laboratories of many semiconductor manufacturers and telecommunications equipment manufacturers have been working hard on the development of micro-mirror arrays (MMA). Their first applications were

in digital projection equipment, which has now expanded into digital cinema projectors, with sometimes more than two million micro-mirrors per chip switching at frequencies of up to 66 kHz [60]. Later these MMAs were used on telescopes to enhance fuzzy images, and studies are underway to use them for the next generation space telescope and for a multi space object spectrometer [61]. Recently MMAs are finding applications in the telecommunications market as optical multiplexers and cross-connect switches. Most MMAs are fabricated from silicon and thus fall into the general category of Micro-Electro-Mechanical-Systems (MEMS). The size of an MMA mirror is usually less than a mm across, it requires very low power to move, and it can move fast - typically in milliseconds.

The first generation of MMAs was binary, which meant that the micro-mirrors could only assume two positions. In the last few years a new generation of MMAs is being introduced, which are equipped with servo control. These are sometimes referred to as *scanning MMAs* (SMMA), because the micro-mirror tilt angle is a function of the input command signal [62]. These SMMAs are available in array topologies. The size of the micro-mirrors is in micrometer scale, and they have an octagonal shape. The micro-mirrors are driven by electrostatic actuators, which are located behind the reflecting front facet of the mirrors. By modulating the voltage of the mirror pads about the bias level it is possible to generate controlled rotations of the micro-mirrors. The range of rotation is a few degrees, which corresponds to a laser beam rotation that is twice as large. The resonant frequencies of the micr-mirrors are in order of few kHz.

Micro-mirror arrays could prove a very useful technology for LADAR sensors. Micro-mirrors can act as a distributed scanner that generates a large number of micro-beams, which can scan the workspace from different angles and positions.

An alternative use of the micro-mirror arrays could be that of an optical switch that routes a laser beam to various optical fibers, which then become the generators of the LADAR beam scanning action. There are various techniques to split laser beams with arrays of micro-scanners and to generate micro-beams that can scan in many directions from different locations [55]. In terrain locations where sharp transitions exist, directed scanning from multiple micro-scanners of overlapping workspaces can be used to increase the mapping resolution. The terrain observations should be collected by the same controller and combined to provide a high-resolution 3D image of the scene (stitching or registering procedure) [55].

Many industrial companies are working now on creating sophisticated laser ranging systems, be it mobility LADAR for unoccupied ground vehicles, control of construction machinery, gaming gesture control or inspection of manufacturing processes. The above research towards small, inexpensive, accurate, and fast LADAR systems is relevant to all these applications.

Bibliography

[1] Denny, M., *Blip, Ping & Buss*, Johns Hopkins University Press, Baltimore, MD, 2007.

[2] Houston, J. D., and Carswell, A. I., "Four-component polarization measurement of lidar atmospheric scattering," *Appl. Optics* **17**(4), pp. 614–620, 1978.

[3] Griffen, M., "Complete Stokes parameterization of laser backscattering from artificial clouds," M.S. thesis, University of Utah, Salt Lake City, UT, 1983.

[4] Sassen K., "LiDAR backscatter depolarization techniques for cloud and aerosol research," *Light Scattering by Nonspherical Particles: Theory, Measurements, and Geophysical Applications*, Mishchenko, M. I., Hovenier, J. W., and Travis, I. D., (Eds.), Academic Press, San Diego, CA, p. 393– 416, 2000.

[5] M. I. Skolnick (Ed.), *RADAR Handbook*, McGraw-Hill, New York (1970).

[6] Donald, R., Wehner, "High-resolution Radar", Artech House Inc., 1987.

[7] Alongi, Anthony V., "Short Pulse and Wide Bandwidth High-resolution Radars", *Proceedings of the NATO Advanced Study Institute*, held in Goslar, Sep 22- Oct 03, 1975.

[8] Barton and Ward "Hand Book of Radar Measurement", Prentice-Hall Inc., Englewood Cliffs, New Jersey, 1969.

[9] Rihaczek, A. W., "Principles of High-Resolution Radar", McGraw-Hill, New York, 1969.

[10] Bernfeld, M, and Cook, C. E., "Radar Signals: An Introduction to Theory and Application", Academic Press Inc., London, 1967.

[11] Skolnik, Merrill I., "Radar Hand Book", McGraw Hill, New Delhi, 2008.

[12] Richards, Mark A., "Fundamentals of Radar Signal Processing", Tata McGraw-Hill, New Delhi, 2005.

[13] Peebles, Peyton Z., Jr., "Radar Principles", John Wiley & Sons (ASIA) Ltd, Sigapore, 2004.

[14] Agrawal, G. P., *Fiber-Optic Communications Systems, Third Edition*, New York: John Wiley & Sons, 2002.

[15] Levanon, N., and Mozeson, E., "Radar Signals", Hoboken, NJ: J. Wiley & Sons, 2004.

[16] Richmond, R. D., and Cain, S. C., Direct-detection LADAR systems, Bellingham, WA: *SPIE Press*, 2010.

[17] Amann, M.C., Bosch, T., Lescure, M., Myllylä, R., and Rioux, M., “Laser ranging: a critical review of usual techniques for distance measurement,” *Opt. Eng*. vol. 40, pp. 10–19, 2001.

[18] Albota, M. A., Heinrichs, R. M., Kocher, D. G., Fouche, D. G., Player, B. E., OBrien, M. E., Aull, B. F., Zayhowski, J. J., Mooney, J., Willard, B C., and Carlson, R. R., "Three-dimensional imaging laser radar with a photon-counting avalanche photodiode array and microchip laser," *Appl. Opt*. vol. 41, pp. 7671-7678, 2002.

[19] Dierking, M.P., and Duncan, B.D., "Periodic, pseudonoise waveforms for multifunction coherent ladar," *Appl. Opt*. vol. 49, pp. 1908-1922, 2010.

[20] Beck, S. M., Buck, J. R., Buell, W.F., Dickinson, R. P., Kozlowski, D. A., Marechal, N. J., and Wright, T.J., "Synthetic-aperture imaging laser radar: laboratory demonstration and signal processing," *Appl. Opt*. vol. 44, pp. 7621-7629, 2005.

[21] Dieckmann, A., "FMCW-LIDAR with tunable twin-guide laser diode," *Electron. Lett.*, vol. 30, pp. 308–309 ,1994.

[22] Nakamura, K., Hara, T., Yoshida, M., Miyahara, T., and Ito, H., "Optical frequency domain ranging by a frequency-shifted feedback laser," *IEEE J. Quantum Electron.*,vol. 36,pp. 305–316 2000.

[23] Amann, M.C., "Phase-noise limited resolution of coherent LIDAR using widely tunable laser diodes," *Electron. Lett.*, vol. 28,pp. 1694–1696, 1992.

[24] Economou, G., Youngquist, R. C., and Davies, D. E. N., "Limitations and noise in interferometric systems using frequency ramped singlemode diode lasers," *J. Lightwave Technol*. vol .4, pp. 1601–1608, 1986.

[25] Goodman, J. W., *Statistical Optics*, Wiley, New York, 1985.

[26] Woodward, P. M., “Probability and Information Theory with Applications to Radar”, Pergamon Press, Oxford, 1953.

[27] Edde, B., “Radar Principles, Technology, Applications”, Prentice Hall PTR, Upper Saddle River, NJ, 1995.

[28] Mahafza, Baseem R., “Radar Systems Analysis and Design Using MATLAB”, CRC Press, 2000.

[29] Nathanson F. E., “Radar Design Principles”, 2nd ed., Prentice Hall of India, New Delhi, 2004.

[30] Barker, R. H., “Group Synchronization of Binary Digital Systems”, Communication Theory (*Proc. of the 2nd London Symposium on Information Theory*), London, Butterworth’s, 1953, pp. 273-287.

[31] Turyn, R., “Optimum Codes Study”, contract AF19 (604)-5473, *Sylvania Electronic Systems final report*, January 1960.

[32] M.J.E. Golay, "Complementary series," *IRE Trans. On Information Theory,* vol. 7, pp. 82-87, 1961.

[33] Golomb, S. W., and Scholtz, R. A., “Generalized Barker Sequences”, *IEEE Trans. on Information Theory*, vol. 11, no. 4, October 1965, pp. 533-537.

[34] Friese, M., “Polyphase Barker Sequences upto Length 36”, *IEEE Trans. on Information Theory*, vol. 42, no. 4, July 1996, pp.1248-1250.

[35] Borwein, P., and Ferguson, R., “Polyphase Sequence with Low Autocorrelation”, *IEEE Trans. on Information Theory*, vol. 51, no. 4, Apr 2005, pp. 1564-1567.

[36] Frank, R. L., “Polyphase Codes with Good Non-periodic Correlation Properties”, *IEEE Trans. on Information Theory*, vol. 9, no. 1, Jan 1963, pp. 43-45.

[37] Chu, D. C., “Polyphase Codes with Good Periodic Correlation Properties”, *IEEE Trans. on Information Theory*, vol. 18, no. 4, July 1972, pp. 531-533.

[38] Lewis, B. L., and Krestschmer, F. F., “A New Class of Polyphase Pulse Compression Codes and Techniques”, *IEEE Trans. on Aerospace and Electronic Systems*, vol. AES-17, no. 3, May 1981a, pp. 364-372.

[39] Lewis, B. L., and Krestschmer, F. F., “Linear Frequency Modulation Derived Polyphase Pulse Compression Codes”, *IEEE Trans. on Aerospace and Electronic Systems*, vol. AES-18, no. 5, September 1982, pp. 673-641.

[40] Boehmer, A. M., “Binary Pulse Compression Codes”, *IEEE Trans. on Information Theory*, vol. 13, no. 2, April 1967.

[41] Goley, M. J. E., “A Class of Finite Binary Sequences with Alternate Autocorrelation Values Equal to Zero”, *IEEE Trans. on Information Theory*, vol. 18, May 1972, pp. 449-450.

[42] Bomer L., and Antweiler, M., “Polyphase Barker Sequences”, *Electronic Letters*, vol. 25, no. 23, Nov 1989, pp. 1577-1579.

[43] Boztas, S., Hammons, R., and Kumar P. V., “4-Phase Sequences with Near Optimum Correlation Properties”, *IEEE Trans. on Information Theory*, vol. 38, no. 3, May 1992, pp.1101-1113.

[44] Kravitz D., Grodensky D., Levanon N., and Zadok A., “High-Resolution Low-Sidelobe Laser Ranging Based on Incoherent Pulse Compression,” *IEEE Photonics Technology Letters*, vol. 24 no. 23, pp. 2119-2121, Dec. 2012.

[45] Litsyn, S., *Peak Power Control in Multicarrier communications*. Cambridge, UK: Cambridge University Press, 2007.

[46] Borwein P. B., and Ferguson, R. A., "A complete description of Golay pairs for length up to 100," *Mathematics of Computation*, vol.**73**, pp. 967-985, 2004.

[47] Nazarathy, M., "Real-Time Long Range Complementary Correlation Optical Time Domain Reflectometer," *Journal of Lightwave Technology*, vol. 45, 1, Jan. 1989.

[48] Levanon, N. "Noncoherent pulse compression", *IEEE Transactions on Aerospace and Electronic Systems*, 42, 2, pp. 756-765,Apr. 2006.

[49] Kravitz, D., Grodensky, D., Zadok, A., and Levanon, N., "Incoherent compression of complementary code pairs for laser ranging and detection," *Proceedings of IEEE International Conference on Microwaves, Communications, Antennas and Electronics Systems*, COMCAS, 2013.

[50] Soto, M., and Le Floch, S., and Thevanez, L., "Bipolar optical pulse coding for performance enhancement in BOTDA sensors," *Optics Express*, vol. 21, pp. 16390-16397, 2013.

[51] Antman, Y., and Yaron L., and Langer, T., and Tur, and M., Levanon, N., and Zadok, A., "Experimental demonstration of localized Brillouin gratings with low off-peak reflectivity established by perfect Golomb codes," *Optics Letters*, vol. 38, pp. 4701-4704, 2013.

[52] Peer, U., and Levanon, N., "Compression waveforms for non-coherent radar," *IEEE Radar Conference*, 2007, Boston, MA, pp. 17-20, Apr. 2007.

[53] Harris F., "On the use of windows for harmonic analysis with the discrete Fourier transform," *Proceedings of the IEEE*, vol. **66**, pp. 51–83, 1978.

[54] Klinger O., "Long Microwave-Photonic Variable Delay of Chirped Waveforms", *M.S. thesis*, Dept. Elect. Eng., Bar-Ilan Univ., Ramat-Gan, Israel, 2012.

[55] Stone W., Juberts M., Dagalakis N., Stone J., and Gorman J. (Eds.), "Performance Analysis of Next-Generation LADAR for Manufacturing, Construction, and Mobility," *NISTIR 7117*, National Institute of Standards and Technology, Gaithersburg, MD (2004).

[56] Jau L., and Lee Y., "Optical code-division multiplexing systems using Manchester coded Walsh codes," *IEE Proceedings on Optoelectronics*, vol. 151, pp. 81-86, 2004.

[57] Levanon N., "Noncoherent radar pulse compression based on complementary sequences", *IEEE Trans. on Aerospace and Electronic Systems*, vol. 45, pp. 742-747, 2009.

[58] Andrews, L., and Phillips, R., "Laser beam propagation through random media", *SPIE Optical Engineering Press*, Bellingham, WA., 1998.

[59] Burton, R., Schott, J., and Brown, S., "Elastic LADAR Modeling for Synthetic Imaging Applications", SPIE Proceedings, vol. 4816, pp. 144-155, July 2002.

[60] Younse, J., "Projection Display Systems Based on the Digital Micromirror Device," *Proceedings of Micromechanical structures and Microelectromechanical Devices for Optical Processing and Multimedia Applications*, p. 64, October 1995.

[61] Zamkotsian F., Gautier J., and Lanzoni P., "Characterization of MOEMS devices for the instrumentation of next generation space telescope", *Proc. SPIE 4980, Reliability, Testing, and Characterization of MEMS/MOEMS II*, 324, January 2003.

[62] Dagalakis, N., LeBrun, T., and Lippiatt, J., "Micro-mirror array control of optical tweezer trapping beams", *Proceedings of the 2002 2nd IEEE Conference on Nanotechnology*, 2002.

[63] Amatucci, E., Dagalakis, N., Kramar, J., Scire, F., "Performance Evaluation of a Parallel Cantilever Biaxial Micropositioning Stage," *American Society of Precision Engineering*, 15th Annual Meeting 2000, Scottsdale, Arizona, October 2000.

[64] Boone, B., Bokulic, R., Andrews, G., McNutt, Jr., R., Dagalakis, N., "Optical and Microwave Communications System Conceptual Design for a Realistic Interstellar Explorer," *47th SPIE Meeting*, Seattle, WA., July 2002.

[65] Gottlieb, M., Ireland, C., Ley, J., "Electro-Optic and Acousto-Optic Scanning and Deflection," Marcel Dekker Publisher, 1983.

[66] Langer, D., Mettenleiter, M., Hartl, F., Frohlich, C., "Imaging ladar for 3-D surveying of real world environments," *International Journal of Robotic Research*, Vol. 19, No. 11, pp. 1075-1088, 2000.

Appendix A

Autocorrelations of coded sequences

Barker13 (Peak = 13):

T = [+1 +1 +1 +1 +1 -1 -1 +1 +1 -1 +1 -1 +1]

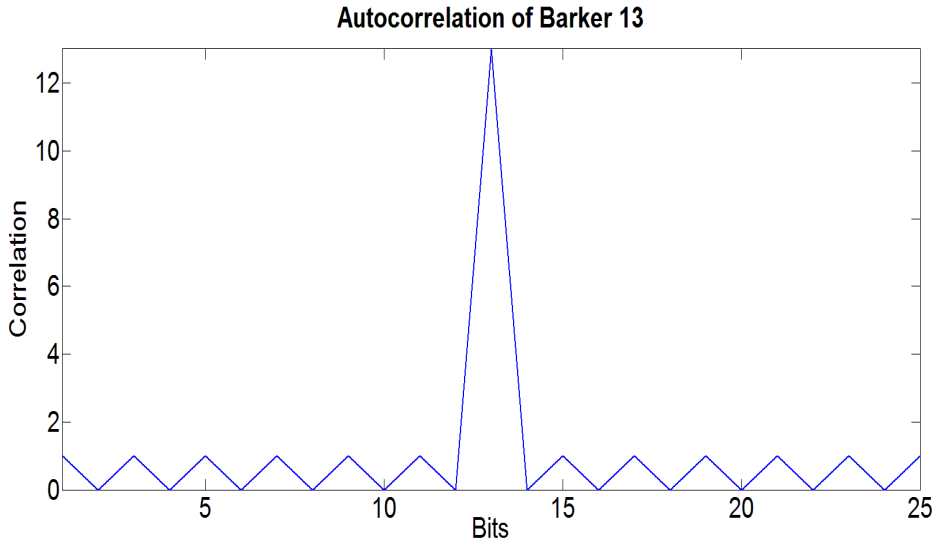

Figure A1. Autocorrelation of Barker 13 code.

MPSL82 (Peak = 82):

T= [+1 +1 +1 +1 -1 -1 +1 -1 +1 +1 -1 -1 +1 -1 -1 +1 -1 +1 +1 +1 -1 +1 -1 -1 +1 +1+1 -1 -1 -1 -1 -1 -1 -1 +1 +1 -1 -1 +1 +1 +1 -1 -1 -1 +1 +1 +1 -1 +1 +1 -1 +1 +1 +1-1 +1 +1+1 -1 +1 +1 -1 -1 +1 -1+1 -1 +1 +1 -1 +1 -1 -1 +1 -1 +1 -1 +1 +1 +1 +1 +1]

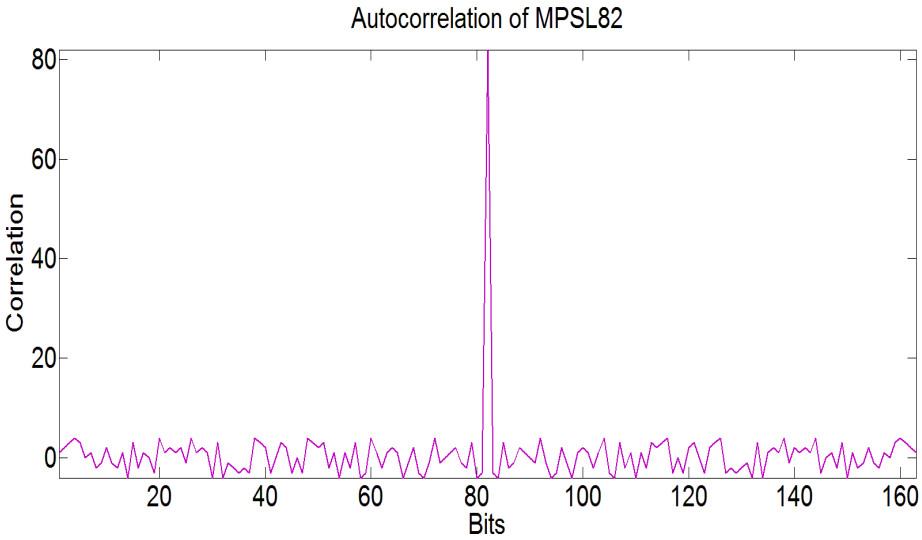

Figure A2. Autocorrelation of MPSL82 code.

MPSL1112 (Peak = 1112):

The 1112 bits-long MPSL sequence is proprietary of Prof. Levanon, and cannot be specified here. Its auto-correlation trace is given below as indication of its favorable sidelobe properties.

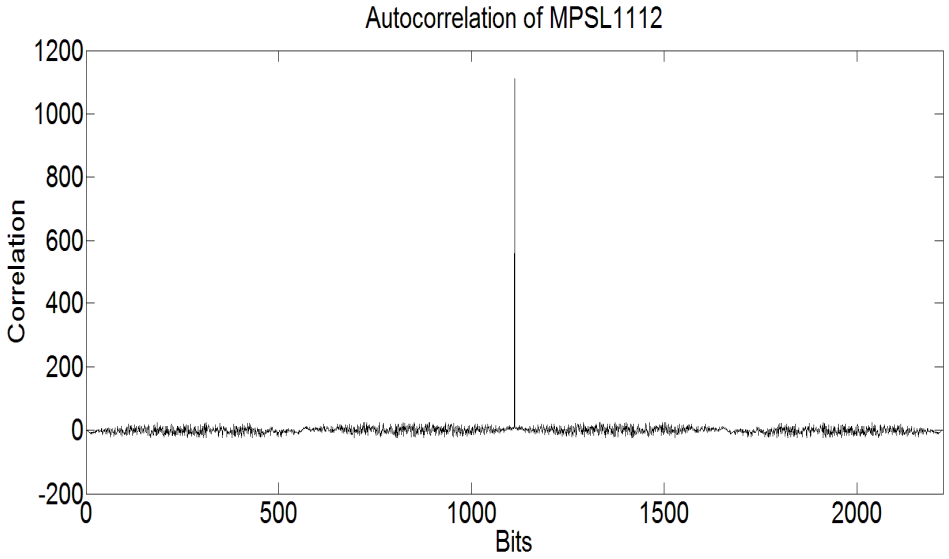

Figure A3. Autocorrelation of MPSL1112 code.

Golay416 (Peak = 832 – twice number of bits):

T = [-1 -1 -1 +1 +1 -1 -1 -1 +1 -1 +1 +1 -1 +1 -1 +1 -1 +1 +1 -1 -1 +1 -1 -1 -1 -1-1-1 -1 -1 +1 -1 -1 +1
+1 -1 +1 -1 -1-1 -1 -1 +1 -1 +1 +1 +1 -1 -1 +1 +1 +1-1 -1 -1 +1 +1 -1 -1 -1 +1 -1 +1 +1 -1+1 -1 +1 -1
+1 +1 -1 -1 +1 -1 -1 -1 -1+1 +1 +1 +1 -1 +1 +1 -1 -1 +1 -1 +1 +1+1 +1 +1 -1 +1 -1 -1 -1 +1 +1 -1 -1 -
1-1 -1 -1 +1 +1 -1 -1 -1 +1 -1 +1 +1 -1 +1 -1 +1 -1 +1 +1 -1 -1 +1 -1 -1 -1 -1-1 -1 -1 -1 +1 -1 -1 +1 +1 -
1 +1 -1 -1 -1 -1 -1 +1 -1 +1 +1 +1 -1 -1 +1 +1 +1+1 +1 +1 -1 -1 +1 +1 +1 -1 +1 -1 -1 +1-1 +1 -1 +1 -1
-1 +1 +1 -1 +1 +1 +1 +1 -1 -1 -1 -1 +1 -1 -1 +1 +1 -1 +1 -1 -1 -1 -1 -1 +1 -1 +1 +1 +1 -1 -1 +1 +1 +1 -
1 -1 -1+1 +1 -1 -1 -1 +1 -1 +1 +1 -1+1 -1 +1 -1 +1 +1 -1 -1 +1 -1 -1 -1 -1-1 -1 -1 -1 +1 -1 -1 +1 +1 -1
+1 -1 -1-1 -1 -1 +1 -1 +1 +1 +1 -1 -1 +1 +1 +1 -1 -1 -1 +1 +1 -1 -1 -1 +1 -1 +1 +1 -1 +1 -1 +1 -1 +1 +1
-1 -1 +1 -1 -1 -1 -1+1 +1 +1 +1 -1 +1 +1 -1 -1 +1 -1 +1 +1 +1+1 +1 -1 +1 -1 -1 -1 +1 +1 -1 -1 -1+1 +1
+1 -1 -1 +1 +1 +1 -1 +1 -1 -1 +1 -1 +1 -1 +1 -1 -1 +1 +1 -1 +1 +1 +1 +1+1 +1 +1 +1 -1 +1 +1 -1 -1 +1
-1 +1 +1 +1 +1 +1 -1 +1 -1 -1 -1 +1 +1 -1 -1 -1 -1 -1 -1 +1 +1 -1 -1 -1 +1 -1 +1 +1 -1 +1 -1 +1 -1 +1
+1 -1 -1 +1 -1 -1 -1 -1 +1 +1 +1 +1 -1 +1 +1 -1 -1 +1 -1 +1 +1 +1 +1 +1 -1 +1 -1 -1 -1 +1 +1 -1 -1 -1 -
1 -1 -1 +1 +1 -1 -1 -1 +1 -1 +1 +1 -1 +1 -1 +1 -1 +1 +1 -1 -1 +1 -1 -1 -1 -1 -1 -1 -1 +1 -1 -1 +1 +1 -1
+1 -1 -1 -1 -1 -1 +1 -1 +1 +1 +1 -1 -1 +1 +1 +1 -1 -1 -1 +1 +1 -1 -1 -1 +1 -1 +1 +1 -1 +1 -1 +1 -1 +1
+1 -1 -1 +1 -1 -1 -1 -1 +1 +1 +1 +1 -1 +1 +1 -1 -1 +1 -1 +1 +1 +1 +1 +1 -1 +1 -1 -1 -1 +1 +1 -1 -1 -1 -
1 -1 -1 +1 +1 -1 -1 -1 +1 -1 +1 +1 -1 +1 -1 +1 -1 +1 +1 -1 -1 +1 -1 -1 -1 -1 -1 -1 -1 +1 -1 -1 +1 +1 -1
+1 -1 -1 -1 -1 -1 +1 -1 +1 +1 +1 -1 -1 +1 +1 +1+1 +1 +1 -1 -1 +1 +1 +1 -1 +1 -1 -1 +1 -1 +1 -1 +1 -1 -
1 +1 +1 -1 +1 +1 +1 +1 -1 -1 -1 -1 +1 -1 -1 +1 +1 -1 +1 -1 -1 -1 -1 -1 +1 -1 +1 +1 +1 -1 -1 +1 +1 +1 +1
+1 +1 -1 -1 +1 +1 +1 -1 +1 -1 -1 +1-1 +1 -1 +1 -1 -1 +1 +1 -1 +1 +1 +1 +1 +1 +1 +1 +1 -1 +1 +1 -1 -1
+1 -1 +1 +1+1 +1 +1 -1 +1 -1 -1 -1 +1 +1 -1 -1 -1+1 +1 +1 -1 -1 +1 +1 +1 -1 +1 -1 -1 +1 -1 +1 -1 +1 -
1 -1 +1 +1 -1 +1 +1 +1 +1 -1 -1 -1 -1 +1 -1 -1 +1 +1 -1 +1 -1 -1 -1 -1 -1 +1 -1 +1 +1 +1 -1 -1 +1 +1 +1
-1 -1 -1 +1 +1 -1 -1 -1 +1 -1 +1 +1 -1 +1 -1 +1 -1 +1 +1 -1 -1 +1 -1 -1 -1 -1 -1 -1 -1 +1 -1 -1 +1 +1 -
1 +1 -1 -1 -1 -1 -1 +1 -1 +1 +1 +1 -1 -1 +1 +1 +1 +1 +1 +1 -1 -1 +1 +1 +1 -1 +1 -1 -1 +1 -1 +1 -1 +1 -1
-1 +1 +1 -1 +1 +1 +1 +1 -1 -1 -1 -1 +1 -1 -1 +1 +1 -1 +1 -1 -1 -1 -1 -1 +1 -1 +1 +1 +1 -1 -1 +1 +1 +1]

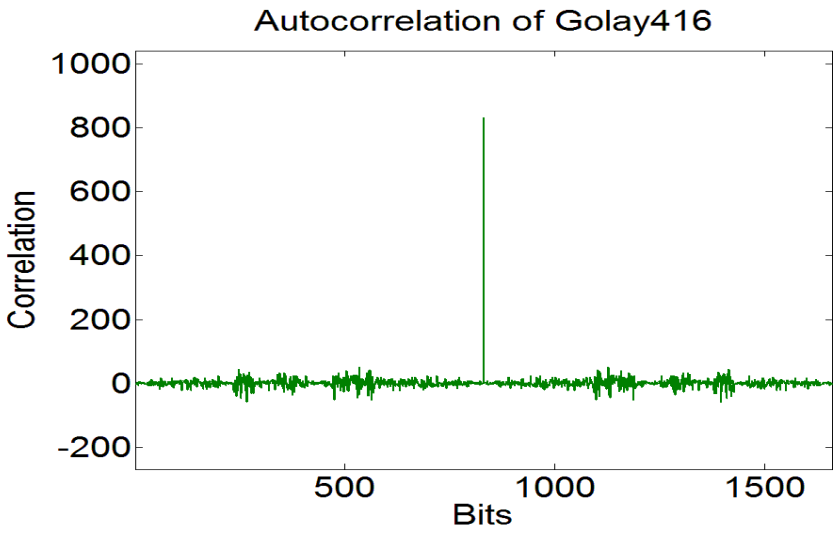

Figure A4. Autocorrelation of Golay416 code.

תוכן העניינים

תקציר

מדידות טווח ברזולוציה גבוהה הינן בעלות חשיבות רבה ליישומים אזרחיים כמו גם ליישומים צבאיים. בהשווה לשימוש בגלי רדיו ומיקרו-גלים במערכות מכ״מ, גלים בתחום האופטי המשמשים כיום למדידות טווח במערכות לייזר יכולים לשאת אותות בעלי רוחבי סרט גדולים יותר ובכך לאפשר מדידות ברזולוציה גבוהה יותר. כמו כן, גלים בתדרים אופטיים מיסודם חסינים יותר בפני הפרעות אלקטרומגנטיות הדדיות, ויכולים להיות מופצים בקלות ולמרחק רב על-גבי סיבים אופטיים.

יצירתם ושידורם של פולסים קצרים בעלי הספק גבוה הינם קשים למימוש במערכות מעשיות, ועלולים להוות סיכון בטיחותי. בנוסף, השימוש בפולסים קצרים אשר לאחריהם פרקי זמן ארוכים של שקט מביא לירידה באנרגיה הכוללת של האות המשודר, וכתוצאה מכך יחס האות לרעש במדידה מתקלקל. לחילופין, ניתן להשתמש בסדרות ארוכות של מספר רב של פולסים קצרים, בעלות הספקים רגעיים נמוכים אולם אנרגיה כוללת גבוהה, בצירוף טכניקות דחיסה מתאימות. עיבוד באמצעות אוטו-קורלציה, או מסננת מתואמת, של אותות וסדרות ממושכים עשוי לדחוס את כל האנרגיה שלהם לתוך אונה מרכזית צרה ורבת-עוצמה, עם אונות צד נמוכות. משום כך, טכניקה זו מאפשרת לשחזר את הרזולוציה הגבוהה ורעש הרקע הנמוך המתקבלים בשימוש בפולס קצר ועוצמתי, בתוספת יתרונות משמעותיים: ההספק הרגעי של סדרות ארוכות יכול להיות נמוך בכמה סדרי גודל, דבר המאפשר יצירה פשוטה ובטיחותית יותר של האותות ובנוסף מקשה על האזנה ושיבוש מצד גורם עויין.

מטרת עבודה זו הינה מדידות טווח ברזולוציה גבוהה באמצעות קידוד פוטוני של אותות לייזר, ודחיסה של אותות ארוכים. מערכת מד טווח הלייזר המוצעת משתמשת בסדרות מקודדות ועיבוד מתאים על מנת לאפשר מדידות טווח ברזולוציה גבוהה עם אונות צד נמוכות. ברוב המקרים הנידונים בספרות, שיטות דחיסה יעילות מחייבות שימוש בקודי פאזה, כאשר קידוד עוצמה נותן ביצועים פחותים. ואולם, מדידת הפאזה במערכות אופטיות מצריכה שימוש במקלטים קוהרנטיים מסובכים ליישום. לחילופין, אנו משתמשים בשיטת דחיסה לא קוהרנטית חדשנית אשר פותחה לאחרונה על ידי פרופ׳ נדב לבנון מאוניברסיטת תל אביב. בשיטה זו, קודי פאזה דו-קוטביים מומרים לקודי עוצמה חד-קוטביים, באמצעות אלגוריתם לקידוד מיקום, ולאחר מכן משמשים לאיפנון מקור הלייזר. האותות המוחזרים ממטרה נדגמים על ידי גלאי עוצמה, ולאחר מכן עוברים קורלציה עם קוד דו-קוטבי אשר שמור בזכרון המקלט באופן ספרתי.

אף על פי שתהליך השידור והקליטה אינם קוהרנטיים, תוצאת הקורלציה משחזרת כמעט לחלוטין את אונות הצד הנמוכות המתקבלות בשימוש בקוד הפאזה הדו-קוטבי המקורי.

מד טווח הלייזר המבוסס על דחיסה לא קוהרנטית הודגם באופן נסיוני. ייצוג חד-קוטבי של שני סוגי קודים נבחן נסיונית: 1) קוד המתוכנן לקבלת אונות צד מינימליות, ו- 2) זוג קודים משלימים, ידועים כקודי Golay, אשר מבטלים את אונות הצד אחד של השני. רזולוציות המדידה שהושגה היתה 15 ס״מ במרחק מירבי של 70 מטרים. המרחק למטרה נמדד בהצלחה ביחסי אות לרעש נמוכים, עד ל- 20 dB- (רעש יותר חזק מהאות הרצוי פי 100). טווח המדידה תלוי בהחזר המטרה, והוא עשוי להגיע למאות מטרים באמצעות מיצוע על-פני זמנים קצרים יחסית. תוצאות אלו מציגות לראשונה הדגמה ניסיונית מלאה של עיקרון הדחיסה הלא קוהרנטית במדידות טווח אל משטח מחזיר ״ריאלי״.

העבודה מאורגנת באופן הבא: הקדמה למד טווח לייזר ולדחיסת אותות ארוכים ניתנת בפרק 1. סקרי ספרות הקשורים ליצירת צורות גל מקודדות שונות והשוואה בין ביצועיהם מודגשים בפרק זה. מערכת מד טווח לייזר המבוססת על דחיסה לא קוהרנטית של אותות מפורטת בפרק 2. סימולציות וניסיונות מעבדה ראשוניים למרחק קצר מוצגים אף הם בפרק זה. פרק 3 מוקדש למדידות מרחק עד לטווח של 70 מטרים, אל עבר משטח מחזיר מייצג אשר מפזר את האור הפוגע על-פני טווח זויות רחב. לבסוף, סיכום ודיון לגבי המשך העבודה מופיעים בפרק 4.

עבודת המחקר בוצעה תחת הנחייתו של פרופ' אבי צדוק מהפקולטה להנדסה באוניברסיטת בר-אילן

מדידת טווח לייזר באמצעות שיטות דחיסה לא קוהרנטיות

חיבור לשם קבלת התואר "דוקטור לפילוסופיה"

מאת:

דניאל גרודנסקי

הפקולטה להנדסה

הוגש לסנט של אוניברסיטת בר-אילן

רמת גן **תשרי תשע"ה**